Journal: Monthly Notices of the Royal Astronomical Society
Article doi: 10.1093/mnras/stu1954
Article title: Traces of large-scale dynamo action in the kinematic stage
First Author: Kandaswamy Subramanian
Corr. Author: Kandaswamy Subramanian

INSTRUCTIONS

We encourage you to use Adobe's editing tools (please see the next page for instructions). If this is not possible, please list clearly in an e-mail. Please do not send corrections as track changed Word documents.

Changes should be corrections of typographical errors only. Changes that contradict journal style will not be made.

These proofs are for checking purposes only. They should not be considered as final publication format. The proof must not be used for any other purpose. In particular we request that you: do not post them on your personal/institutional web site, and do not print and distribute multiple copies. Neither excerpts nor all of the article should be included in other publications written or edited by yourself until the final version has been published and the full citation details are available. You will be sent these when the article is published.

1. **Licence to Publish:** Oxford Journals requires your agreement before publishing your article. If you haven't already completed this, please sign in with your My Account information and complete the online licence form. Details on how to do this can be found in the Welcome to Oxford Journals email.
2. **Permissions: Permission to reproduce any third party material in your paper should have been obtained prior to acceptance. If your paper contains figures or text that require permission to reproduce, please inform me immediately by email.**
3. **Author groups:** Please check that all names have been spelled correctly and appear in the correct order. Please also check that all initials are present. Please check that the author surnames (family name) have been correctly identified by a pink background. If this is incorrect, please identify the full surname of the relevant authors. Occasionally, the distinction between surnames and forenames can be ambiguous, and this is to ensure that the authors' full surnames and forenames are tagged correctly, for accurate indexing online.
4. **Figures:** If applicable, figures have been placed as close as possible to their first citation. Please check that they are complete and that the correct figure legend is present. Figures in the proof are low resolution versions that will be replaced with high resolution versions when the journal is printed.
5. **Missing elements:** Please check that the text is complete and that all figures, tables and their legends are included.
6. **Special characters and equations:** Please check that special characters, equations and units have been reproduced accurately.
7. **URLs:** Please check that all web addresses cited in the text, footnotes and reference list are up-to-date.
8. **Funding:** If applicable, any funding used while completing this work should be highlighted in the Acknowledgements section. Please ensure that you use the full official name of the funding body.

AUTHOR QUERIES - TO BE ANSWERED BY THE CORRESPONDING AUTHOR

The following queries have arisen during the typesetting of your manuscript. Please answer these queries by marking the required corrections at the appropriate point in the text.

Query No.	Nature of Query	Author's Response
Q1	Author: The figures have been processed according to information entered by you during the submission of your manuscript. Please note that if you have confirmed that you wish to publish your figures in colour in print and that you are willing to pay the £200 (+VAT) charge, you will be invoiced upon publication. Black and white versions of figures are provided at the end of the paper. Please check the black and white versions to assess their quality for the print version of the journal, and contact us if you have any concerns.	
Q2	Author: To check that we have your surnames correctly identified and tagged (e.g. for indexing), we have coloured pink the names that we have assumed are surnames. If any of these are wrong, please let us know so that we can amend the tagging.	
Q3	Author: If you refer to any data bases in your paper, please note the journal policy for properly crediting those responsible for compiling the data base. Rather than citing only a URL, if at all possible please also cite a reference (and include it in the reference list), or if a reference is not available then the names of those who compiled the data base. Note that some data bases do provide guidelines on how they should be cited – please check for these and follow them in your paper where appropriate.	
Q4	Author: The MNRAS list of approved key words has been revised and updated. The new list is appended to these proofs. If you had previously selected key words from the old list, please now check them carefully against the new list in case they need to be changed, or there are new ones that you would like to add. If you had not previously selected key words from the MNRAS approved list, please now choose up to six from the new list.	
Q5	Author: Please note that it is journal style to refer to 'our' Galaxy with a capital 'G' (e.g. in case of Galaxy, Galactic Centre or Galactocentric) and to other galaxies with a lowercase 'g'. Please check that all the notations in this paper are correct.	
Q6	Author: When used to mean the numerical value '3.14', the Greek letter 'pi' must always be written in roman (i.e. 'π' rather than 'π'). Please check all the notations throughout the text carefully.	
Q7	Author: Journal style rules state that vectors and tensors must be written in bold italic ($\boldsymbol{X}$), matrices must be written in bold san serif ($\mathbf{X}$) and scalars must be written in italic (X). Please check carefully that the notations used throughout this paper are correct.	
Q8	Author: Please note that computer software/programming languages must be styled in SMALL CAPITAL LETTERS, according to journal style. Please check and correct this paper accordingly.	
Q9	Author: Please check the figures in the PDF proof carefully.	

Query No.	Nature of Query	Author's Response
Q10	Author: As per journal style, the running head short title of a paper must not exceed 45 characters (including spaces between words and punctuation marks); please supply an alternative short title of up to 45 characters (including any spaces between words and punctuation marks) that can be used instead.	
Q11	Author: In this article, both terms 'k_s' and 'k^s' have been used. Please suggest whether these mean the same and one of them should be retained throughout, or they are okay as given. Kindly check for some more instances in this paper.	
Q12	Author: Reference 'Sur et al. (2008)' is not cited in text. Please check.	

MAKING CORRECTIONS TO YOUR PROOF

These instructions show you how to mark changes or add notes to the document using the Adobe Acrobat Professional version 7.0 (or onwards) or Adobe Reader 8 (or onwards). To check what version you are using go to **Help** then **About**. The latest version of Adobe Reader is available for free from get.adobe.com/reader.

For additional help please use the **Help** function or, if you have Adobe Acrobat Professional 7.0 (or onwards), go to http://www.adobe.com/education/pdf/acrobat_curriculum7/acrobat7_lesson04.pdf

Displaying the toolbars

Adobe Reader 8: Select Tools, Comments & Markup, Show Comments and Markup Toolbar**. If this option is not available, please let me know so that I can enable it for you.**

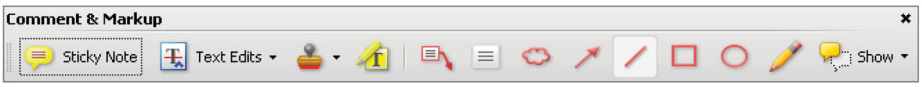

Acrobat Professional 7: Select Tools, Commenting, Show Commenting Toolbar**.**

Adobe Reader 10: To edit the galley proofs, use the Comment Toolbar (Sticky Note and Highlight Text).

Using Text Edits

This is the quickest, simplest and easiest method both to make corrections, and for your corrections to be transferred and checked.

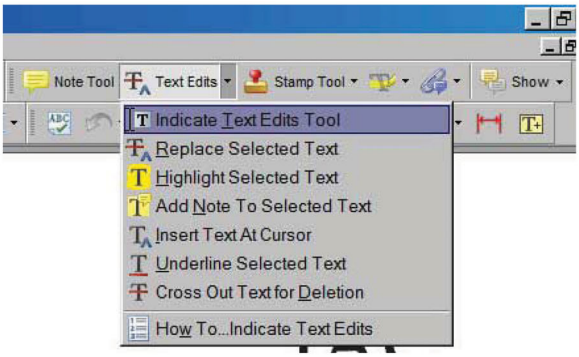

1. Click **Text Edits**
2. Select the text to be annotated or place your cursor at the insertion point.
3. Click the **Text Edits** drop down arrow and select the required action.

   You can also right click on selected text for a range of commenting options.

Pop up Notes

With *Text Edits* and other markup, it is possible to add notes. In some cases (e.g. inserting or replacing text), a pop-up note is displayed automatically.

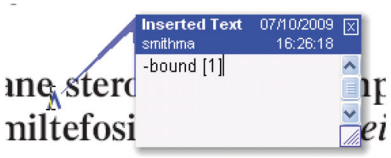

To **display** the pop-up note for other markup, right click on the annotation on the document and selecting **Open Pop-Up Note**.

To **move** a note, click and drag on the title area.

To **resize** of the note, click and drag on the bottom right corner.

To **close** the note, click on the cross in the top right hand corner.

To **delete** an edit, right click on it and select **Delete**. The edit and associated note will be removed.

SAVING COMMENTS

In order to save your comments and notes, you need to save the file (**File, Save**) when you close the document.
A full list of the comments and edits you have made can be viewed by clicking on the Comments tab in the bottom-left-hand corner of the PDF.

Traces of large-scale dynamo action in the kinematic stage

Kandaswamy Subramanian[1]★ and Axel Brandenburg[2,3]

[1]*Inter University Centre for Astronomy and Astrophysics, Post Bag 4, Pune University Campus, Ganeshkhind, Pune 411 007, India*
[2]*Nordita, KTH Royal Institute of Technology and Stockholm University, Roslagstullsbacken 23, SE-10691 Stockholm, Sweden*
[3]*Department of Astronomy, AlbaNova University Center, Stockholm University, SE-10691 Stockholm, Sweden*

Accepted 2014 September 15. Received 2014 September 12; in original form 2014 August 19

ABSTRACT

Using direct numerical simulations (DNS), we verify that in the kinematic regime, a turbulent helical dynamo grows in such a way that the magnetic energy spectrum remains to high-precision shape-invariant, i.e. at each wavenumber k the spectrum grows with the same growth rate. Signatures of large-scale dynamo action can be identified through the excess of magnetic energy at small k, of one of the two oppositely polarized constituents. Also a suitably defined planar average of the magnetic field can be chosen such that its rms value isolates the strength of the mean field. However, these different means of analysis suggest that the strength of the large-scale field diminishes with increasing magnetic Reynolds number $\mathrm{Re_M}$ like $\mathrm{Re_M^{-1/2}}$ for intermediate values and like $\mathrm{Re_M^{-3/4}}$ for larger ones. Both an analysis from the Kazantsev model including helicity and the DNS show that this arises due to the magnetic energy spectrum still peaking at resistive scales, even when helicity is present. As expected, the amplitude of the large-scale field increases with increasing fractional helicity, enabling us to determine the onset of large-scale dynamo action and distinguishing it from that of the small-scale dynamo. Our DNS show that, contrary to earlier results for smaller scale separation (only 1.5 instead of now 4), the small-scale dynamo can still be excited at magnetic Prandtl numbers of 0.1 and only moderate values of the magnetic Reynolds numbers (∼160).

Key words: dynamo – magnetic fields – MHD – turbulence – Sun: dynamo – galaxies: magnetic fields.

1 INTRODUCTION

The origin of large-scale magnetic fields in astrophysical bodies such as stars and galaxies remains an outstanding problem, given that those fields are coherent on the scale of the systems themselves. Indeed, the observed scale is often larger than the scale of the turbulent motions, which would be the convective scale in the Sun or the turbulent length-scales induced by supernova remnants in galaxies. These large-scale magnetic fields are typically explained as being due to turbulent dynamo action, whereby the combined action of helical turbulence and shear amplifies and maintains fields coherent on scales larger than the scales of random stirring. We refer to this as the large-scale or mean-field dynamo. However, when the magnetic Reynolds number, $\mathrm{Re_M}$, is large, such turbulent motions also generically lead to the small-scale or fluctuation dynamo, whereby magnetic fields coherent on scales of the order of or smaller than the outer scales of the turbulence are rapidly generated. In the following, we use mean-field and fluctuation dynamos synonymously with large-scale and small-scale dynamos, respectively.

Typically, the growth rate of the fluctuation or small-scale dynamo is much larger than the growth rate associated with the mean-field or large-scale dynamo. Then, in a system where both types of dynamos can in principle operate, at least in the kinematic stage, magnetic fluctuations generated by the fluctuation dynamo would in principle rapidly overwhelm the large-scale field which could be generated by mean-field dynamo action. The question then arises, whether in such a system there is any evidence for large-scale fields at all in the kinematic stage.

Large-scale dynamo action from helical turbulence has clearly been seen in several direct numerical simulations (DNS) during the late non-linear stage when the magnetic field is close to saturation (e.g. Brandenburg 2001). This is partially due to the phenomenon of 'self-cleaning', which means the suppression of power on scales between the largest and the driving scale of the turbulence. However, during the early phase, there is no clear evidence for large-scale dynamos, especially when small-scale dynamo action is also expected to be possible.

Small-scale dynamo action is best studied in the case when there is no helicity (see Brandenburg & Subramanian 2005a, for a review). In the presence of helicity, however, not only the large-scale dynamo may become possible, but also the small-scale dynamo might get

★ E-mail: kandu@iucaa.ernet.in

modified such that large-scale and small-scale dynamos are just different aspects of a single dynamo (Subramanian 1999).

It is instructive to think of the kinematic small-scale dynamo problem as a quantum mechanical potential problem, where by the existence of bound states in the potential, corresponds to growing modes of the small-scale dynamo (Kazantsev 1968). An extension of this picture in the presence of helicity is that the corresponding potential allows for 'tunnelling' of these bound states into 'free-particle' states (Subramanian 1999; Brandenburg & Subramanian 2000; Boldyrev et al. 2005). The larger growth rate of the small-scale dynamo, compared to that of the large-scale dynamo, is then reflected in the fact that the potential well at the scale, say l, where the bound state is located, is deeper than the scale where the free-particle states exist, say L. In case there is only a single fastest growing eigenfunction, which grows fastest during the kinematic state, this change in the potential depths at scales l and L could then reflect itself in the corresponding strength of the eigenfunction, which would have a larger amplitude on the scale l than the scale L, or corresponding wavenumbers proportional to l^{-1} and L^{-1}. Whether this picture is indeed a useful description of the kinematic eigenfunction is currently unknown.

Our aim here is to examine whether in helical turbulence there is evidence for the existence of the large-scale dynamo even in the presence of the fluctuation dynamo. To isolate features of the large-scale dynamo, we consider here, for most part, the regime of small magnetic Prandtl numbers, $\mathrm{Pr_M} = \nu/\eta$, where ν is the kinematic viscosity and η the magnetic diffusivity. For small values of $\mathrm{Pr_M}$, e.g. for $\mathrm{Pr_M} = 0.1$, the small-scale dynamo is expected to be much harder to excite if there were no helicity in the flow (Iskakov et al. 2007). The large-scale dynamo, on the other hand, is known to be virtually independent of $\mathrm{Pr_M}$ and $\mathrm{Re_M}$ once $\mathrm{Re_M} > O(1)$; see Brandenburg (2009) and Malyshkin & Boldyrev (2010). One then expects this to provide a better chance of seeing evidence for the large-scale field in the kinematic stage.[1] However, as we will see below, even this small $\mathrm{Pr_M}$ case does not yield a decisive change, in preferentially hosting a large-scale dynamo.

We restrict ourselves to the study of subsonic flows with Mach numbers around 0.3. While this is relevant to stars that also have small values of $\mathrm{Pr_M}$, larger Mach numbers would be interesting and relevant to the study of the warm and cold components of the interstellar medium, but this has the problem that it results in the possibility of shocks. This would force us to increase the viscosity, resulting in smaller values of the Reynolds number. It is well known that in supersonic flows, the small-scale dynamo is harder to excite (Haugen, Brandenburg & Mee 2004b; Federrath et al. 2011; Schober et al. 2012; Schleicher et al. 2013), but the large-scale dynamo, which is the subject of the present study, depends essentially on the scale separation ratio of the turbulence and may not (or only weakly) depend on the Mach number. For example, supernova-driven turbulence in galaxies, involving flows at high Mach number, has been shown to be capable of driving a large-scale dynamo (Gressel et al. 2008a,b; Gent et al. 2013a,b).

We begin by presenting the basic equations of our DNS (Section 2), discuss then the results for different magnetic Reynolds and Prandtl numbers (Section 3), and place them within the framework of a unified analytical model (Section 4), before concluding in Section 5.

[1] This is reminiscent of ideas by Tobias & Cattaneo (2013) and Cattaneo & Tobias (2014), where strong shear suppresses small-scale dynamo action and then allows large-scale dynamo waves to persist at high $\mathrm{Re_M}$ in their helical flow models.

2 MODEL

We consider dynamo action in a cubic domain of size L_1^3, driven by turbulence forced at wavenumbers $k_\mathrm{f} \approx 4\,k_1$, where $k_1 = 2\pi/L_1$ is the smallest wavenumber in the domain. The forcing is assumed to be helical, so that one can in principle have the operation of an α^2 type large-scale dynamo. To begin with, as explained above, we consider a small value of the magnetic Prandtl number $\mathrm{Pr_M} = 0.1$.

We solve the compressible hydromagnetic equations:

$$\frac{\partial}{\partial t}\boldsymbol{A} = \boldsymbol{u}\times\boldsymbol{B} - \eta\mu_0\boldsymbol{J}, \tag{1}$$

$$\frac{\mathrm{D}}{\mathrm{D}t}\boldsymbol{u} = -c_\mathrm{s}^2\nabla\ln\rho + \frac{1}{\rho}\boldsymbol{J}\times\boldsymbol{B} + \boldsymbol{F}_\mathrm{visc} + \boldsymbol{f}, \tag{2}$$

$$\frac{\mathrm{D}}{\mathrm{D}t}\ln\rho = -\nabla\cdot\boldsymbol{u}, \tag{3}$$

where $\boldsymbol{A}$ is the magnetic vector potential, $\boldsymbol{u}$ the velocity, $\boldsymbol{B}$ the magnetic field, η the molecular magnetic diffusivity, μ_0 the vacuum permeability, $\boldsymbol{J}$ the electric current density, c_s the isothermal sound speed, ρ the density, $\boldsymbol{F}_\mathrm{visc}$ the viscous force, $\boldsymbol{f}$ the helical forcing term, and $\mathrm{D}/\mathrm{D}t = \partial/\partial t + \boldsymbol{u}\cdot\nabla$ the advective time derivative. The viscous force is given as $\boldsymbol{F}_\mathrm{visc} = \rho^{-1}\nabla\cdot 2\nu\rho\boldsymbol{S}$, where ν is the kinematic viscosity, and $\boldsymbol{S}$ is the traceless rate of strain tensor with components $\boldsymbol{S}_{ij} = \frac{1}{2}(u_{i,j} + u_{j,i}) - \frac{1}{3}\delta_{ij}\nabla\cdot\boldsymbol{u}$. Commas denote partial derivatives.

The energy supply for a helically driven dynamo is provided by the forcing function $\boldsymbol{f} = \boldsymbol{f}(\boldsymbol{x}, t)$, which is random in time and defined as

$$\boldsymbol{f}(\boldsymbol{x}, t) = \mathrm{Re}\{N\boldsymbol{f}_{\boldsymbol{k}(t)}\exp[\mathrm{i}\boldsymbol{k}(t)\cdot\boldsymbol{x} + \mathrm{i}\phi(t)]\}, \tag{4}$$

where $\boldsymbol{x}$ is the position vector. The wavevector $\boldsymbol{k}(t)$ and the random phase $-\pi < \phi(t) \le \pi$ change at every time step, so $\boldsymbol{f}(\boldsymbol{x}, t)$ is δ-correlated in time. Therefore, the normalization factor N has to be proportional to $\delta t^{-1/2}$, where δt is the length of the time step. On dimensional grounds it is chosen to be $N = f_0 c_\mathrm{s}(|\boldsymbol{k}|c_\mathrm{s}/\delta t)^{1/2}$, where f_0 is a non-dimensional forcing amplitude. We choose $f_0 = 0.02$, which results in a maximum Mach number of about 0.3 and an rms velocity of about 0.085, which is almost the same for all the runs. At each time step we select randomly one of many possible wavevectors in a certain range around a given forcing wavenumber with average value k_f. Transverse helical waves are produced via (Haugen, Brandenburg & Dobler 2004a)

$$\boldsymbol{f}_{\boldsymbol{k}} = \boldsymbol{R}\cdot\boldsymbol{f}_{\boldsymbol{k}}^{(\mathrm{nohel})} \quad \text{with} \quad \boldsymbol{R}_{ij} = \frac{\delta_{ij} - \mathrm{i}\sigma\epsilon_{ijk}\hat{k}_k}{\sqrt{1+\sigma^2}}, \tag{5}$$

where σ is a measure of the helicity of the forcing and $\sigma = 1$ for positive maximum helicity of the forcing function and

$$\boldsymbol{f}_{\boldsymbol{k}}^{(\mathrm{nohel})} = (\boldsymbol{k}\times\hat{\boldsymbol{e}})/\sqrt{\boldsymbol{k}^2 - (\boldsymbol{k}\cdot\hat{\boldsymbol{e}})^2} \tag{6}$$

is a non-helical forcing function, where $\hat{\boldsymbol{e}}$ is an arbitrary unit vector not aligned with $\boldsymbol{k}$; note that $|\boldsymbol{f}_{\boldsymbol{k}}|^2 = 1$ and

$$\boldsymbol{f}_{\boldsymbol{k}}\cdot(\mathrm{i}\boldsymbol{k}\times\boldsymbol{f}_{\boldsymbol{k}})^* = 2\sigma k/(1+\sigma^2), \tag{7}$$

so the relative helicity of the forcing function in real space is $2\sigma/(1+\sigma^2)$.

Table 1. Summary of runs discussed in this paper.

Run	$\mathrm{Re_M}$	$\mathrm{Pr_M}$	σ	$\tilde{\lambda}$	N
A01	1	0.1	1	−0.004	128^3
B01	3	0.1	1	0.014	128^3
C01	16	0.1	1	0.029	128^3
D01	33	0.1	1	0.033	256^3
E01	65	0.1	1	0.036	256^3
F01	160	0.1	1	0.038	256^3
F02	160	0.2	1	0.038	256^3
F05	160	0.5	1	0.041	256^3
F07	160	0.7	1	0.045	256^3
F1	160	1	1	0.051	256^3
G01	340	0.1	1	0.040	1024^3
G02	360	0.2	1	0.037	1024^3
G05	330	0.5	1	0.050	512^3
G1	330	1	1	0.069	256^3
F01b	160	0.1	0.7	0.032	256^3
F01c	160	0.1	0.5	0.023	256^3
F01d	160	0.1	0.3	0.010	256^3
F01e	160	0.1	0.2	0.005	512^3
F01f	160	0.1	0.1	0.003	512^3
f005	160	0.05	0	0.001	512^3
g005	310	0.05	0	0.015	512^3
f01	160	0.1	0	0.003	512^3
g01	200	0.1	0	0.006	512^3
e02	80	0.2	0	−0.003	256^3
f02	160	0.2	0	0.015	256^3
d05	30	0.5	0	−0.004	128^3
e05	80	0.5	0	0.016	128^3
d1	40	1	0	0.010	128^3
e1	60	1	0	0.019	128^3
f1	150	1	0	0.045	128^3

Our model is governed by several non-dimensional parameters. In addition to the scale separation ratio k_f/k_1, introduced above, there are the magnetic Reynolds and Prandtl numbers

$$\mathrm{Re_M} = u_\mathrm{rms}/\eta k_\mathrm{f}, \quad \mathrm{Pr_M} = \nu/\eta. \tag{8}$$

These two numbers also define the fluid Reynolds number, $\mathrm{Re} = u_\mathrm{rms}/(\nu k_\mathrm{f}) = \mathrm{Re_M}/\mathrm{Pr_M}$. The maximum values that can be attained are limited by the numerical resolution and become more restrictive at larger scale separation. The calculations have been performed Q8 using the PENCIL CODE[2] at resolutions between 128^3 and 1024^3 mesh points.

3 SIMULATIONS

In the following, we present runs at different values of $\mathrm{Re_M}$, $\mathrm{Pr_M}$, and σ; see Table 1.

3.1 Growth rate

It turns out that for helical driving, and $\mathrm{Pr_M} = 0.1$, the onset of Q9 dynamo action occurs at small values of $\mathrm{Re_M}$; see Fig. 1, where we show the normalized growth rate, $\lambda/u_\mathrm{rms}k_\mathrm{f}$, of a dynamo as a function of $\mathrm{Re_M}$. We see that, for $k_\mathrm{f}/k_1 = 4$, the critical value of $\mathrm{Re_M}$ is around 2. Furthermore, the increase of λ becomes less steep for $\lambda/u_\mathrm{rms}k_\mathrm{f} \gtrsim 0.03$, which is a value that was found earlier for fully helical large-scale dynamos (Brandenburg 2009), who also used $k_\mathrm{f}/k_1 = 4$.

[2] http://pencil-code.googlecode.com

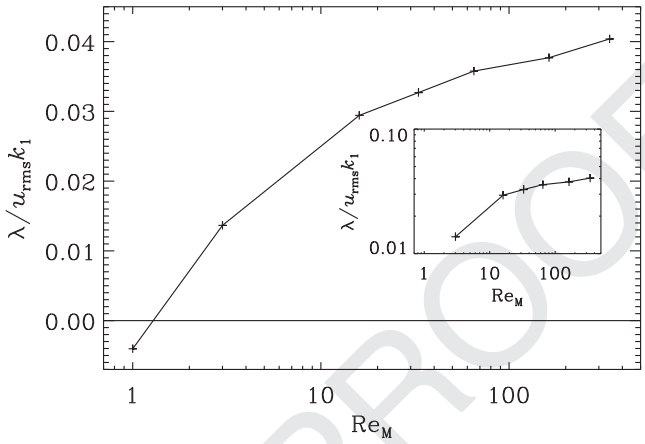

Figure 1. Normalized growth rate versus $\mathrm{Re_M}$ for $\mathrm{Pr_M} = 0.1$ and $\sigma = 1$. For intermediate values of $\mathrm{Re_M}$ below 100, the growth rate corresponds to that of a helical large-scale dynamo. The inset shows $\lambda/u_\mathrm{rms}k_\mathrm{f}$ versus $\mathrm{Re_M}$ in double-logarithmic representation.

3.2 Wavenumber-dependent growth rate

One of the features that we want to examine is whether the magnetic field grows as an eigenfunction in the kinematic stage, when both large- and small-scale dynamo action is possible. For this we look at the time evolution of magnetic energy spectra, $E_\mathrm{M}(k,\,t)$. It is convenient to represent the time evolution in the form

$$E_\mathrm{M}(k,\,t) = E_\mathrm{M0}(k)\,\mathrm{e}^{2\lambda(k)t}. \tag{9}$$

Since $E_\mathrm{M0}(k)$ depends on the initial magnetic field strength, B_ini, it is convenient to write it as

$$E_\mathrm{M0}(k) = \tfrac{1}{2}B_\mathrm{ini}^2\mathcal{E}_\mathrm{M}(k), \tag{10}$$

where $\mathcal{E}_\mathrm{M}(k)$ is the normalized spectrum with $\int \mathcal{E}_\mathrm{M}(k)\,\mathrm{d}k = 1$. Note that we have here allowed for a k-dependent growth rate, $\lambda(k)$. This enables us to assess quantitatively to what extent the growth rate depends on k. The resulting $\lambda(k)$ is shown in the bottom panel of Fig. 2 for $\mathrm{Pr_M} = 0.1$ and $\mathrm{Pr_M} = 1$, respectively. We see that, to very good accuracy, the growth rate is the same for different wavenumbers, confirming that the spectra grow as one eigenfunction, even when both large-scale and small-scale dynamos are possible, due to helical forcing.

3.3 Magnetic spectra in the polarization basis

For the α^2 dynamo, which arises in helical turbulence, due to magnetic helicity conservation, one expects the helicity of small-scale and large-scale fields to have different signs at early times. Thus, one would be able to see a clearer signature of the large-scale field, if one looks separately for positively and negatively polarized helical fields, defined as

$$E_\mathrm{M}^\pm(k,\,t) = \tfrac{1}{2}\left[E_\mathrm{M}(k,\,t) \pm \tfrac{1}{2}kH_\mathrm{M}(k,\,t)\right]. \tag{11}$$

Again, we fit the resulting spectra to an exponential growth, analogous to equation (9), and plot the normalized magnetic energy spectra $\mathcal{E}_\mathrm{M}^\pm(k)$. They are shown in the top panels of Fig. 3 for $\mathrm{Pr_M} = 0.1$, and Fig. 4 for $\mathrm{Pr_M} = 1$. We see that there is indeed excess power

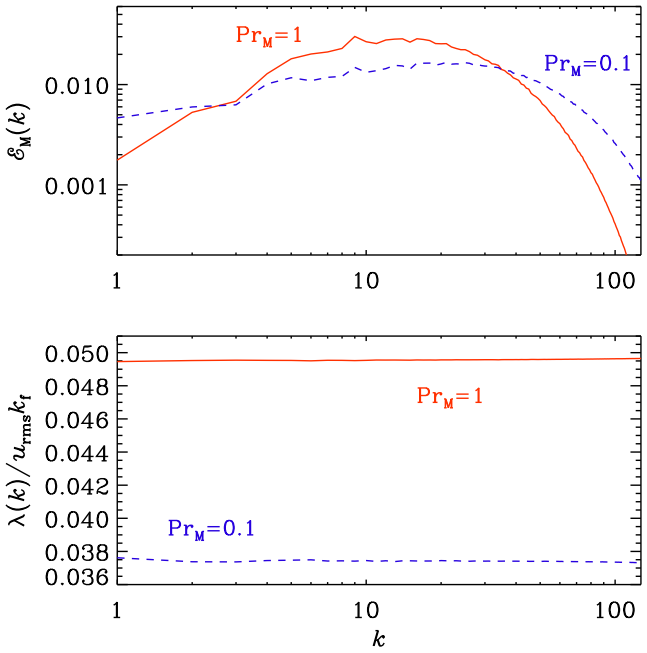

Figure 2. Spectrum of magnetic energy during the kinematic phase for $\mathrm{Pr_M} = 0.1$ (Run F01; blue, dashed lines, $B_{\rm ini} \approx 4 \times 10^{-31}$) and $\mathrm{Pr_M} = 1$ (Run F1; red, solid lines, $B_{\rm ini} \approx 2 \times 10^{-35}$) using $\sigma = 1$ in both cases. The corresponding growth rates as a function of k are given in the bottom panel.

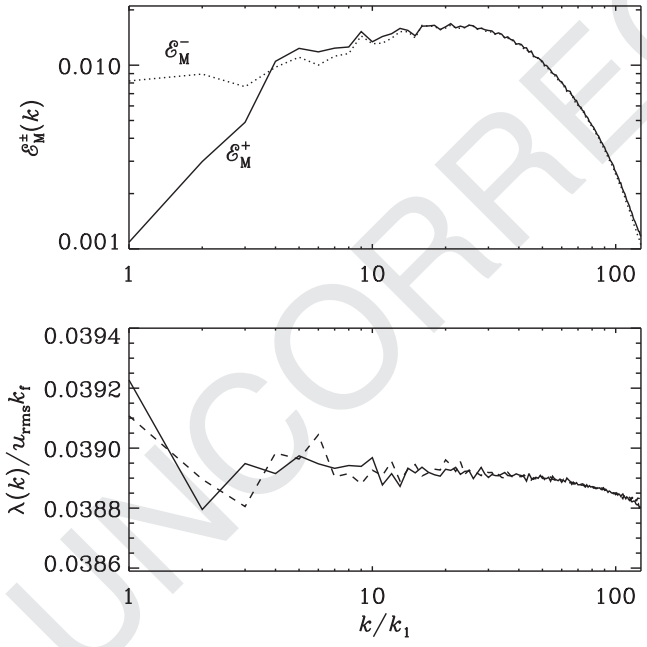

Figure 3. Spectrum of positively and negatively polarized contributions during the kinematic phase for Run F01 with $\sigma = 1$, $\mathrm{Pr_M} = 0.1$, and $\mathrm{Re_M} \approx 160$. The growth rate is given separately for the spectra of magnetic energy of positively (solid line) and negatively (dotted line) polarized contributions.

in $E_{\rm M0}^-$ at small k corresponding to the large-scale field generated in such helical turbulence. For Run F1 with $\mathrm{Pr_M} = 1$, there is also a short range with Kazantsev $k^{3/2}$ scaling. On the other hand, for $\mathrm{Pr_M} = 0.1$ the scaling is significantly flatter, as can be seen from Fig. 5, where we show the result for Run G01 with $\mathrm{Re_M} \approx 330$. Since $\mathrm{Pr_M} = 0.1$, we have here $\mathrm{Re} = 3300$. Note that there is a small uprise of $\lambda(k)$ at $k = k_1$, which may however be a consequence of the time interval Δt being too short (here, $\lambda \Delta t = 10$, while in all other cases it is at least 30).

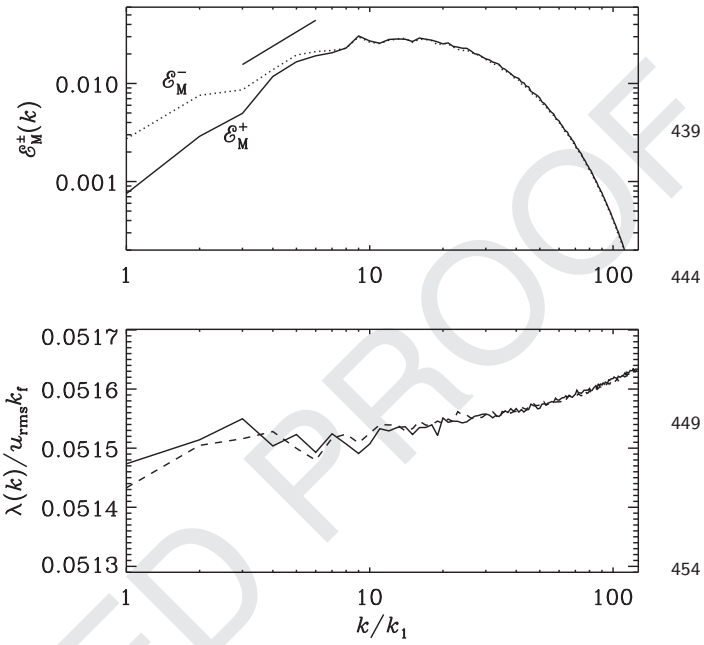

Figure 4. Same as Fig. 3, but for Run F1 with $\sigma = 1$, $\mathrm{Pr_M} = 1$, $\mathrm{Re_M} \approx 160$, and $\mathrm{Pr_M} = 1$. The short straight line gives the $k^{3/2}$ Kazantsev slope for orientation.

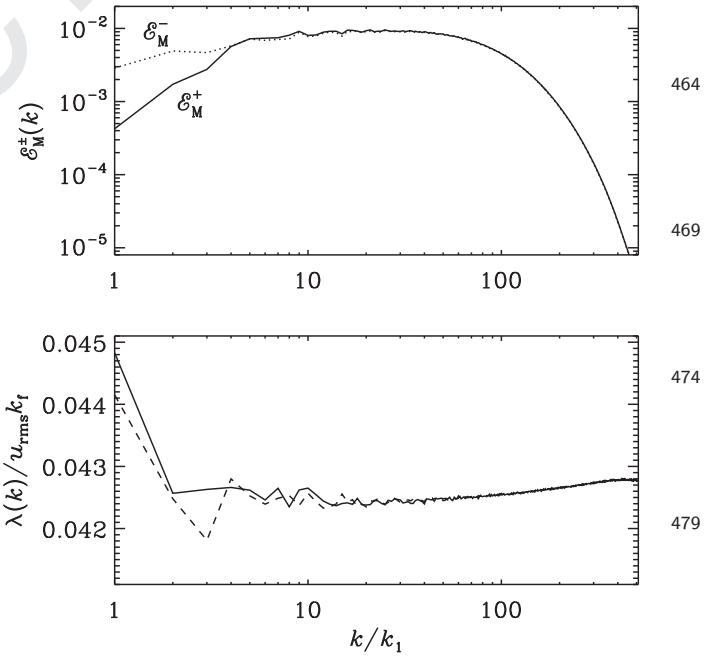

Figure 5. Same as Fig. 3, but for Run G01 with $\sigma = 1$, $\mathrm{Pr_M} = 0.1$, and $\mathrm{Re_M} \approx 330$.

We can see from Figs 3–5 that the magnetic energy spectra rise with k, and peak at wavenumbers much larger than the forcing wavenumber $k_{\rm f}$, and closer to the resistive scale. Therefore, even though there is clear evidence for excess power corresponding to the large-scale field, the rms field is likely to be dominated by small scales, perhaps close to the resistive scale. We will return to this aspect of the kinematic dynamo below.

3.4 Expectation from α^2 dynamos

It is useful to compare the wavenumber of where excess power would occur in an α^2 dynamo. In such a model, the mean magnetic field $\overline{\boldsymbol{B}}$ is governed by the equation

$$\frac{\partial \overline{\boldsymbol{B}}}{\partial t} = \nabla \times (\alpha \overline{\boldsymbol{B}}) + \eta_{\rm T} \nabla^2 \overline{\boldsymbol{B}}, \tag{12}$$

where α characterizes the strength of the α effect and $\eta_{\rm T} = \eta + \eta_{\rm t}$ is the sum of microphysical and turbulent magnetic diffusivities. Solutions proportional to $\exp(\mathrm{i}\boldsymbol{k}\cdot\boldsymbol{x} + \lambda t)$ give the growth rate as $\lambda = |\alpha k| - \eta_{\rm T} k^2$. Its maximum value is attained when $\mathrm{d}\lambda/\mathrm{d}k = 0$, giving the peak at $k_{\rm peak} = |\alpha|/2\eta_{\rm T}$. Based on results of the second-order correlation approximation applied to the high-conductivity limit (Krause & Rädler 1980), one has $\alpha \approx \tau \langle \boldsymbol{\omega} \cdot \boldsymbol{u} \rangle/3$ and $\eta_{\rm t} \approx \tau \langle \boldsymbol{u}^2 \rangle/3$, where $\boldsymbol{\omega} = \nabla \times \boldsymbol{u}$ is the vorticity of the small-scale turbulent flow $\boldsymbol{u}$ and τ is the correlation time. For maximally helical flows, we expect $|\alpha| \approx u_{\rm rms}/3$ and $\eta_{\rm t} \approx u_{\rm rms}/3k_{\rm f}$, so $k_{\rm peak} \approx k_{\rm f}/2$ (Brandenburg, Dobler & Subramanian 2002). Thus, the theoretically expected scale separation is only a factor of 2. This explains that it is in general difficult to identify excess power at the wavenumber $k_{\rm f}/2$ of the α^2 dynamo compared with the wavenumber $k_{\rm f}$ of the turbulence.

Furthermore, the growth rate of the α^2 dynamo is given by substituting $k_{\rm peak}$ into the above expression for λ. We get $\lambda = \lambda_{\rm peak} = |\alpha|^2/4\eta_{\rm T} \sim u_{\rm rms} k_{\rm f}/12 \approx 0.08 u_{\rm rms} k_{\rm f}$. This can be compared with the growth rate obtained in the DNS of $\lambda \sim 0.038 u_{\rm rms} k_{\rm f}$ for ${\rm Pr_M} = 0.1$, ${\rm Re_M} = 160$ case to $\lambda \sim 0.051 u_{\rm rms} k_{\rm f}$ for ${\rm Pr_M} = 1$ case. The smaller value obtained in the DNS perhaps indicates that the field grows less efficiently.

3.5 Growth of planar averages

Another way to isolate the large-scale mean field is to consider horizontal averages of the total magnetic field. We define mean fields as one of three possible planar averages, and determine their rms fields, denoted by

$$\overline{B}^X = \langle \langle \boldsymbol{B} \rangle_{yz}^2 \rangle_x^{1/2},$$
$$\overline{B}^Y = \langle \langle \boldsymbol{B} \rangle_{xz}^2 \rangle_y^{1/2},$$
$$\overline{B}^Z = \langle \langle \boldsymbol{B} \rangle_{xy}^2 \rangle_z^{1/2}. \tag{13}$$

Here, the subscripts behind angle brackets denote the direction over which the average is taken and the capital letter superscript on $\overline{B}$ indicates the direction in which the mean field varies. These averages allow one to isolate the rms values of the eigenfunctions of the α^2 dynamo. The average relevant for our considerations is the one that produces the largest rms value. Which of the three averages it is, is a matter of chance, because the system is statistically isotropic.

In Fig. 6, we show the ratios of the strength of the three mean fields, $\overline{B}^X$, $\overline{B}^Y$, and $\overline{B}^Z$ defined above, to the total rms field as a function of ${\rm Re_M}$, for the case ${\rm Pr_M} = 0.1$ and $\sigma = 1$. We see a fairly strong mean field for ${\rm Re_M} \approx 1$, but as we increase ${\rm Re_M}$, the fractional contribution of the large-scale field during the kinematic phase decreases proportional to ${\rm Re_M^{-1/2}}$; see Fig. 6. For large values of ${\rm Re_M}$, the scaling becomes even steeper. In other words, the magnetic energy of the mean field decreases inversely proportional to ${\rm Re_M}$. Similar scalings for the energy of the mean magnetic field were sometimes expected to occur in the non-linear stage (Vainshtein & Cattaneo 1992), but here it is a property of the dynamo in the linear regime.

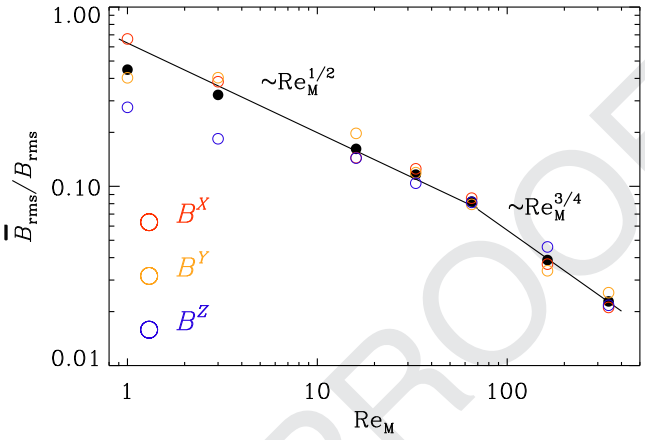

Figure 6. Root-mean-squared value of the mean field relative to that of the total field versus ${\rm Re_M}$ for ${\rm Pr_M} = 0.1$ and $\sigma = 1$ during the kinematic stage. The filled circles denote the averaged DNS results as an average over the contributions from $\overline{B}^X$, $\overline{B}^Y$, and $\overline{B}^Z$. The straight lines correspond to $0.63\,{\rm Re_M^{-1/2}}$ and $1.8\,{\rm Re_M^{-3/4}}$ for lower and larger values of ${\rm Re_M}$, respectively.

We recall that for the present case of a homogeneous α^2 dynamo with periodic boundary conditions the saturation energy is indeed independent of ${\rm Re_M}$, although the time-scale on which such a state is reached increases with time proportional to ${\rm Re_M}$ (Brandenburg 2001; Candelaresi & Brandenburg 2013). We will return to the question of the decreasing strength of the mean magnetic field during the linear stage in Section 4, where we will examine the solutions of the Kazantsev model, generalized to include a helical velocity field (Rogachevskii & Kleeorin 1999; Subramanian 1999; Brandenburg & Subramanian 2000; Boldyrev et al. 2005; Malyshkin & Boldyrev 2007, 2010).

3.6 Dependence on fluid Reynolds number

It is well known that for large ${\rm Pr_M}$ ($\gg$1), the growth rate of the small-scale dynamo scales with Re (asymptotically like ${\rm Re}^{1/2}$; see Schekochihin et al. 2004) and is independent of ${\rm Re_M}$. This is because for ${\rm Pr_M} \gg 1$, the growth rate scales with the eddy turnover rate at the viscous scale, which increases with Re. On the other hand, in the case of small ${\rm Pr_M} \ll 1$, the growth rate scales as the eddy turnover rate at the resistive scale, and hence as ${\rm Re_M^{1/2}}$ (Malyshkin & Boldyrev 2010). We may now ask what happens for fully helical flows with $\sigma = 1$. This is shown in Fig. 7(a), where we show the dependence of λ on Re for ${\rm Re_M} \approx 330$ (Runs G01–G1). Instead, we see actually a weak decline with increasing Re. Furthermore, the fractional strength of the mean field stays fixed; see Fig. 7(b).

3.7 Fractional helicity

As shown above, the onset of large-scale dynamo action occurs at rather small values of ${\rm Re_M}$, but it does require the presence of helicity in the flow. Therefore, the onset of large-scale dynamo action is mainly determined by the amount of helicity, which is quantified by the dynamo number. For an α^2 dynamo, the relevant dynamo number is $C_\alpha = \alpha/\eta_{\rm T0} k_1$, but in DNS this quantity is well approximated by the quantity (Blackman & Brandenburg 2002; Candelaresi & Brandenburg 2013)

$$C_\alpha^{\rm DNS} = \epsilon_{\rm f} k_{\rm f}/k_1, \tag{14}$$

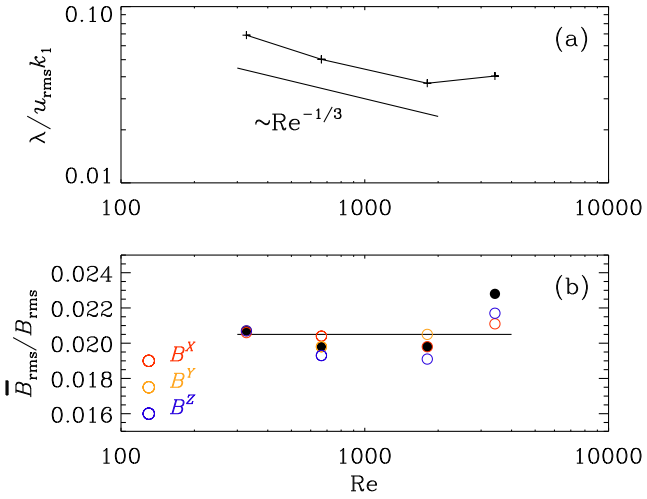

Figure 7. (a) Normalized growth rate versus Re for $\mathrm{Re_M} \approx 330$ and $\sigma = 1$ and (b) root-mean-squared value of the mean field relative to that of the total field during the kinematic stage. Similar to Fig. 6, the filled circles denote the averaged DNS results as an average over the contributions from $\overline{B}^X$, $\overline{B}^Y$, and $\overline{B}^Z$. The horizontal line is shown for reference.

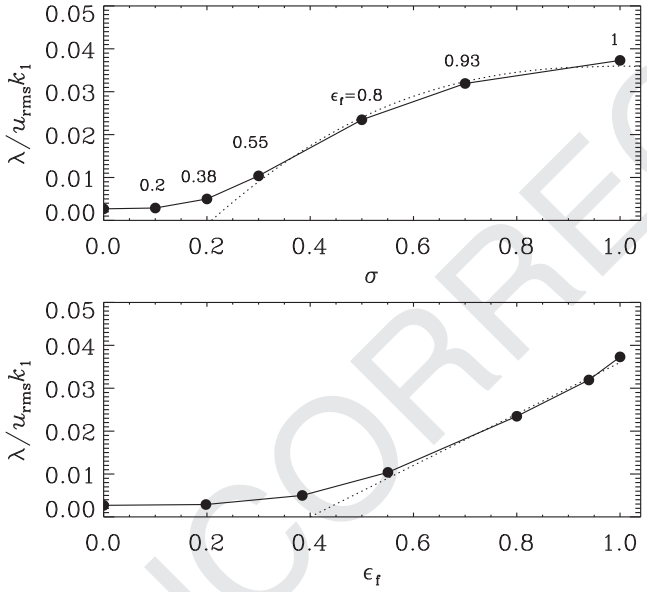

Figure 8. Normalized growth rate versus σ (upper panel, ϵ_f indicated on the data points) and ϵ_f (lower panel), for $\mathrm{Pr_M} = 0.1$ and $\mathrm{Re_M} \approx 160$. The dotted line indicates the tangent and thereby the approximate position of the bifurcation line if the bifurcation was a perfect one.

where k_f/k_1 is the scale separation ratio, $\epsilon_\mathrm{f} = \langle \boldsymbol{\omega} \cdot \boldsymbol{u} \rangle / k_\mathrm{f} u_{\rm rms}^2$ is the fractional helicity, $\boldsymbol{\omega} = \nabla \times \boldsymbol{u}$ is the vorticity, and $u_{\rm rms}$ the rms velocity of the turbulence.

In Fig. 8, we show λ versus σ and ϵ_f. Note that $\epsilon_\mathrm{f} \approx 2\sigma/(1+\sigma^2)$ is obeyed to a good approximation (Candelaresi & Brandenburg 2013). We see that there is an imperfect bifurcation at $\epsilon_\mathrm{f} \approx 0.3$. For large-scale dynamo action to be possible, one needs $C_\alpha > 1$ which requires $\epsilon_\mathrm{f} > k_1/k_\mathrm{f} = 0.25$. The value $\epsilon_\mathrm{f} \approx 0.3$ obtained here is slightly above this theoretical minimum. If one wanted to capture the large-scale dynamo for even smaller ϵ_f, then one requires a smaller k_1/k_f, which implies either a larger box size or a smaller forcing scale.

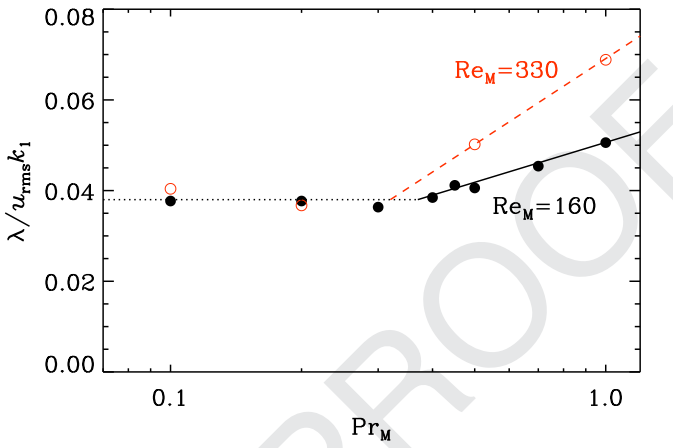

Figure 9. Normalized growth rate versus $\mathrm{Pr_M}$ for $\sigma = 1$, $\mathrm{Re_M} \approx 160$ (Runs F01–F1; solid black line with filled symbols) or ≈330 (Runs G01–G1; dashed red line with open symbols) and varying values of $\mathrm{Re} = \mathrm{Re_M}/\mathrm{Pr_M}$. The dotted line indicates the growth rate for a predominantly large-scale dynamo.

3.8 Transition to small-scale dynamos

Contrary to earlier findings for non-helical turbulence driven at the scale of the domain ($k_\mathrm{f} \approx 1.5$ as opposed to the value 4 used here), the small-scale dynamo is excited even for $\mathrm{Pr_M} = 0.1$. This can be seen from the fact that $\lambda > 0$ even when $\epsilon_\mathrm{f} = 0$; see Fig. 8. Schekochihin et al. (2005) were unable to find small-scale dynamo solutions for $\mathrm{Pr_M} = 0.1$ and later Iskakov et al. (2007) found negative growth rates at $\mathrm{Pr_M} = 0.1$, but positive values for $\mathrm{Pr_M} = 0.05$. This non-monotonic behaviour was associated with the existence of a bottleneck in the kinetic energy spectrum, i.e. a shallower spectrum near the viscous sub-range, where the small-scale dynamo operates. In the non-linear regime, however, no such non-monotonic behaviour is seen (Brandenburg 2011).

As we increase $\mathrm{Re_M}$, the small-scale dynamo becomes more strongly supercritical and the critical value of $\mathrm{Pr_M}$ decreases from 0.4 to 0.3 as we increase $\mathrm{Re_M}$ from 160 to 330; see Fig. 9. Of course, for the fully helical case of this figure, even for $\mathrm{Pr_M} = 0.1$, the dynamo is really a combination of both the large-scale and small-scale dynamos, as we discussed in relation to Fig. 8. In addition, Fig. 9 suggests that the behaviour of the dynamo changes from a mainly large-scale dynamo at small $\mathrm{Pr_M}$ to one that becomes even more strongly controlled by small-scale dynamo action at larger $\mathrm{Pr_M}$.

3.9 $R_\mathrm{m}^\mathrm{crit}$ for the small-scale dynamo at low $\mathrm{Pr_M}$

Early DNS of small-scale dynamos have focused on homogeneous turbulence in a periodic domain where random forcing was applied at the scale of domain, so the forcing wavenumber was typically between 1 and 2 (Haugen et al. 2004a; Schekochihin et al. 2004). In that case, the critical value of $\mathrm{Re_M}$ increased beyond 400 (Schekochihin et al. 2005), but decreased again for smaller values of $\mathrm{Pr_M}$ (Iskakov et al. 2007), which was argued to be a consequence of the bottleneck effect in the kinetic energy spectrum near wavenumber where the small-scale dynamo grows fastest. In non-linear simulations, on the other hand, the bottleneck effect is suppressed and non-linear small-scale dynamo action is sustained at $\mathrm{Pr_M} = 0.1$ for $\mathrm{Re_M} \gtrsim 160$.

Our new work now suggests that this might have been an artefact of an artificially small forcing wavenumber. Our new DNS with

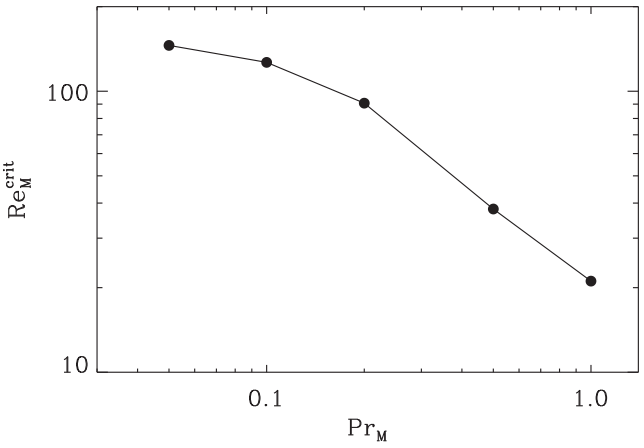

Figure 10. Critical magnetic Reynolds number as a function of magnetic Prandtl number for $k_\mathrm{f} = 4$ and $\sigma = 0$ obtained by interpolating the growth rates of Runs f005–f1 in Table 1.

a forcing wavenumber $k_\mathrm{f} = 4\,k_1$ suggest that small-scale dynamo action is excited at the usual values of Re_M even when $\mathrm{Pr}_\mathrm{M} = 0.1$; see Fig. 10. The reason for this lies probably in the fact that the bottleneck effect is now weaker and that it is connected with particular issues related to the way turbulence is driven. We note that the increase of $R_\mathrm{m}^\mathrm{crit}$ with decreasing Pr_M (Fig. 10) is qualitatively similar to that obtained from the Kazantsev model by Malyshkin & Boldyrev (2010); see the $h = 0$ curve in their fig. 2.

4 INTERPRETATION IN TERMS OF THE KAZANTSEV MODEL WITH HELICITY

In order to interpret and further enhance the results from the DNS, it is instructive to look at the Kazantsev model with helicity (Vainshtein & Kitchatinov 1986; Subramanian 1999; Brandenburg & Subramanian 2000, 2005a; Boldyrev et al. 2005; Malyshkin & Boldyrev 2007, 2010). In this model, the velocity is assumed to be a statistically isotropic, homogeneous random field, and δ-correlated in time. The two-point spatial correlation function of the velocity field can be written as $\langle v_i(\boldsymbol{x},t)v_j(\boldsymbol{y},s)\rangle = T_{ij}(r)\delta(t-s)$, where $r = |\boldsymbol{r}|$ with $\boldsymbol{r} = \boldsymbol{x} - \boldsymbol{y}$ and

$$T_{ij}(r) = \left(\delta_{ij} - \frac{r_i r_j}{r^2}\right) T_\mathrm{N} + \frac{r_i r_j}{r^2}\, T_\mathrm{L} + \epsilon_{ijk} r_k\, F. \qquad (15)$$

Here, $\langle\,\cdot\,\rangle$ denotes averaging over an ensemble of the stochastic velocity field $\boldsymbol{v}$, and we have written the correlation function in a form appropriate for a statistically isotropic and homogeneous tensor (cf. section 34 of Landau & Lifshitz 1987). In equation (15), $T_\mathrm{L}(r)$, $T_\mathrm{N}(r)$, and $F(r)$ are, respectively, the longitudinal, transverse, and helical parts of the correlation function for the velocity field. For an incompressible velocity field, $T_\mathrm{N} = (1/2r)[\mathrm{d}(r^2 T_\mathrm{L})/\mathrm{d}r]$. The magnetic field $\boldsymbol{B}$ is also assumed to be a statistically isotropic, homogeneous random field. Its equal-time, two-point correlation, $M_{ij}(r,t)$, is given by

$$M_{ij} = \left(\delta_{ij} - \frac{r_i r_j}{r^2}\right) M_\mathrm{N} + \frac{r_i r_j}{r^2}\, M_\mathrm{L} + \epsilon_{ijk} r_k\, C, \qquad (16)$$

where $M_\mathrm{L}(r,t)$ and $M_\mathrm{N}(r,t)$ are the longitudinal and transverse correlation functions of the field, and $C(r,t)$ represents the contribution from current helicity to the two-point correlation. Since $\nabla\cdot\boldsymbol{B} = 0$, $M_\mathrm{N}(r,t) = (1/2r)[\partial(r^2 M_\mathrm{L})/\partial r]$. Using the induction equation, the evolution equations for $M_\mathrm{L}(r,t)$ and $C(r,t)$ are given by (Vainshtein & Kitchatinov 1986; Subramanian 1999; Brandenburg & Subramanian 2000, 2005a)

$$\frac{\partial M_\mathrm{L}}{\partial t} = \frac{2}{r^4}\frac{\partial}{\partial r}\left[r^4 \eta_\mathrm{T}\frac{\partial M_\mathrm{L}}{\partial r}\right] + 2G M_\mathrm{L} + 4\alpha C, \qquad (17)$$

$$\frac{\partial H}{\partial t} = -2\eta_\mathrm{T} C + \alpha M_\mathrm{L}, \quad C = -\left(H'' + \frac{4H'}{r}\right), \qquad (18)$$

where primes denote r derivatives and $\eta_\mathrm{T}(r) = \eta + \eta_\mathrm{t}(r)$ is the sum of the microscopic diffusivity η and an effective scale-dependent turbulent magnetic diffusivity $\eta_\mathrm{t}(r) = T_\mathrm{L}(0) - T_\mathrm{L}(r)$. The term $G = -2(T_\mathrm{L}'' + 4T_\mathrm{L}'/r)$ characterizes the rapid generation of magnetic fields by velocity shear and $\alpha(r) = -2[F(0) - F(r)]$ represents the effect of kinetic helicity on the magnetic field. It is related to the usual α effect in mean-field electrodynamics (Moffatt 1978), but it is scale dependent as in Moffatt (1983) and Brandenburg, Rädler & Schrinner (2008).

4.1 Bound states and tunnelling

It is worth recalling some well-known properties of this system; cf. Brandenburg & Subramanian (2005a) and references therein. In the absence of $F(r)$, the system describes the fluctuation or small-scale dynamo. Assuming solutions to be proportional to $\exp(\lambda t)$, the evolution equation for M_L can be transformed to a Schrödinger-type equation, with a potential $U(r)$ depending on T_L, and an energy eigenvalue $E = -\lambda$. Thus, *bound states* in the potential U correspond to growing solutions with $\lambda > 0$. This potential is positive with $U \to 2\eta/r^2 > 0$ as $r \to 0$, while $U \to 2\eta_\mathrm{T0}/r^2 > 0$ as $r \to \infty$, when $T_\mathrm{L}(r) \to 0$. Here, $\eta_\mathrm{T0} = \eta + T_\mathrm{L}(0)$ is the sum of microscopic and turbulent diffusion at large scales. The possibility of growing modes with $\lambda > 0$ is obtained if one can have a potential well with U being sufficiently negative in some intermediate range of r. The growth rate λ is of the order of the fastest eddy turnover rate for a sufficiently supercritical Re_M on this scale. This λ then also gives an estimate of the maximum depth, U_0, of the potential, or $U_0 \sim -\lambda$. The bound state behaviour also implies that the magnetic correlations die away rapidly for scales larger than the correlation scale of the stirring. Kazantsev (1968) also showed that, for a single scale flow (or below the viscous cut-off scale in a large Pr_M turbulent flow), the magnetic power spectrum scales as $E_\mathrm{M}(k) \propto k^{3/2}$, until the resistive cut-off scale, $k_\eta \sim k_\mathrm{f}\mathrm{Re}_\mathrm{M}^{1/2}$, where k_f is again the wavenumber of the energy-carrying eddies. It turns out that the Kazantsev spectrum is preserved, even for a finite correlation time of the velocity field, to the lowest order departures from δ-correlated flow (Bhat & Subramanian 2014). This Kazantsev (1968) result is generalized in Appendix A to include the effect of kinetic helicity of the flow. We will need the resulting asymptotic scaling of $E_\mathrm{M}(k)$ in our arguments below.

In the presence of helical velocity correlations $F(r)$, a remarkable change occurs. The quantity $\alpha(r \to \infty) = -2F(0) \equiv \alpha_0$ is what is traditionally called the α effect. Its presence allows correlations to grow on scales larger than that of the turbulent velocity field, i.e. the large-scale magnetic field (Subramanian 1999). This can easily be seen from equations (17) and (18), where even for $r \to \infty$, we have new generating terms due to the α effect in the form $\dot{M}_\mathrm{L} = \cdots + 4\alpha_0 C$ and $\dot{H} = \cdots + \alpha_0 M_\mathrm{L}$. These couple M_L and C and lead to a growth of large-scale correlations. Indeed for any quasi-stationary states ($\lambda \sim 0$), one finds that the problem of determining the magnetic field correlations once again becomes the problem of determining the zero-energy eigenstate in a modified potential, $U - \alpha^2/\eta_\mathrm{T}$. This potential does not go to zero as $r \to \infty$,

Table 2. Comparing cases I and II.

Type I	SS dynamo dominant LS dynamo seeded by it
Type II	LS dynamo dominant SS dynamo enslaved to it

but instead tends to a negative definite constant $-\alpha_0^2/\eta_{\rm T0}$. So there are strictly no bound states with zero energy/growth rate, for which the correlations vanish sufficiently rapidly at infinity; instead the situation is akin to tunnelling states in quantum mechanics (Subramanian 1999; Brandenburg & Subramanian 2000; Boldyrev et al. 2005; Malyshkin & Boldyrev 2007, 2010).

4.2 Unified growth of large- and small-scale fields

In fact, even when $\lambda \neq 0$, like for the fastest growing modes with growth rates comparable to eddy turnover rates, equations (17) and (18) can be solved exactly in the limit $r \to \infty$. The solution is most transparent for the correlator $w(r,t) = \langle \boldsymbol{B}(\boldsymbol{x},t)\cdot\boldsymbol{B}(\boldsymbol{y},t)\rangle = M_{\rm L} + 2M_{\rm N}$. One finds from fairly straightforward algebra that, for a mode growing with growth rate λ and scale $r \gg l$ (much larger than the turbulent forcing scales),

$$w(r,t) = {\rm e}^{\lambda t}\exp(-k_s r)\frac{A\cos k_{\rm m} r + B\sin k_{\rm m} r}{r} \quad (r \gg l), \tag{19}$$

where

$$k_s = \frac{(2\eta_{\rm T0}\lambda - \alpha_0^2)^{1/2}}{2\eta_{\rm T0}}, \quad k_{\rm m} = \frac{\alpha_0}{2\eta_{\rm T0}}. \tag{20}$$

Note that this solution applies for real k_s, or $\lambda > \alpha_0^2/2\eta_{\rm T0}$, that is for growth rates larger than those of the traditional α^2 dynamo whose maximum growth rate for $\boldsymbol{B}^2$ is also $\alpha_0^2/2\eta_{\rm T0}$; see also Malyshkin & Boldyrev (2007, 2010). This would generically apply if strong small-scale dynamo action is present, that is, when ${\rm Re_M}$ is large enough and, in addition, the eddy turnover rate is bigger than the α^2 dynamo growth rate. However, even in this case, we see that the presence of the large-scale field due to the α effect is evident in the correlator $w(r)$, as reflected in the presence of the oscillating cosine and sine terms in equation (19). In fact, $k_{\rm m} = \alpha_0/2\eta_{\rm T0}$ is exactly the wavenumber for which the growth rate of the mean field α^2 dynamo is maximum, see Section 3.3. This suggests that the fluctuation dynamo, which is amplifying the field at a rate λ, is seeding the simultaneous growth of the large-scale field with a wavenumber $k_{\rm m}$. In other words, the field in this case is growing as one eigenfunction such that the large-scale field is enslaved to the growth of the small-scale field growth. Such a picture is qualitatively consistent with what is found from our DNS for large ${\rm Re_M}$. We will refer to this as Type I, see Table 2.

The presence of a non-zero α_0 can also lead to growth of the field, even when ${\rm Re_M}$ is not large enough to excite the small-scale dynamo. In this situation the α^2 dynamo can be excited, with a continuous spectrum of eigenmodes with $\lambda \le \alpha_0^2/2\eta_{\rm T0}$. The eigenfunction for large $r \gg l$ (i.e. for scales much larger than the turbulent forcing scales) then changes to

$$w(r,t) = {\rm e}^{\lambda t}\frac{A\cos \bar{k}_{\rm m} r + B\sin \bar{k}_{\rm m} r}{r} \quad (r \gg l), \tag{21}$$

where

$$\bar{k}_{\rm m} = \frac{\alpha_0 - (\alpha_0^2 - 2\lambda\eta_{\rm T0})^{1/2}}{2\eta_{\rm T0}}. \tag{22}$$

Again the presence of the large-scale field is evident due to the cosine and sine terms in the correlator $w(r)$. The fastest growing mode in this case has $\lambda = \alpha_0^2/2\eta_{\rm T0}$ and $\bar{k}_{\rm m} \equiv k_{\rm m}$. Moreover, for these solutions the small-scale fields on scales $r < l$ are enslaved to the large-scale dynamo and arise by the velocity field tangling up the large-scale field. Such a solution is what one obtains in our DNS at small $\mathrm{Re_M} < R_{\rm m}^{\rm crit}$. We refer to this case where the large-scale dynamo is dominant as Type II, see Table 2.

4.3 $\mathrm{Re_M}$ dependence of large-scale field strength

The other question is why the large-scale field strength, as measured by the ratio $\overline{B}/B_{\rm rms}$, decreases with ${\rm Re_M}$? It is also somewhat surprising that the large-scale field, decreases with ${\rm Re_M}$ even for moderate ${\rm Re_M} < 100$, especially for ${\rm Pr_M} = 0.1$ when one does not naively expect the small-scale dynamo to operate (Iskakov et al. 2007, see also Fig. 10). There are potentially two effects. First, there could be a decrease of the strength of the eigenfunction, at the scale $r \sim k_{\rm m}^{-1}$, compared to the forcing scale $l \sim k_{\rm f}^{-1}$. This is obtained for Type I, where the small-scale dynamo operates, with the large-scale field enslaved to it. Here, due to the $\exp(-k_s r)$ term in equation (19), the strength of the eigenfunction, at the scale $r \sim k_{\rm m}^{-1}$, would have decreased exponentially by a factor $\sim\exp(-k_s/k_{\rm m})$ from its value at smaller scales. As the ratio $k_s/k_{\rm m}$ increases with increasing growth rate λ, which itself increases with ${\rm Re_M}$ in our simulations, one can obtain a smaller mean field compared to the field at the forcing scale, with increasing ${\rm Re_M}$.

This effect is however not present when the large-scale dynamo is dominant, as the $\exp(-k_s r)$ term is absent in this case (see equation 21). There is however a second effect which is likely to be the more dominant one at large ${\rm Re_M}$ during the kinematic stage in both Types I and II. This is obtained, as we show below, due to the fact that the magnetic power spectrum generically increases further from the forcing wavenumber $k_{\rm f}$ to peak at the resistive one k_η, which itself increases with ${\rm Re_M}$. We discuss this below.

Note that for a purely non-helical small-scale dynamo, the magnetic spectrum in the kinematic stage is expected to increase as $E_{\rm M}(k) \propto k^s$ from the forcing scale $k_{\rm f}$ to the ${\rm Re_M}$-dependent resistive scale, say k_η. In case of a single scale flow, one has the Kazantsev spectrum with, the spectral index $s = 3/2$. What happens when helicity is included, and large-scale field generation becomes possible?

The influence of helicity on the large k behaviour of the magnetic spectrum, for large ${\rm Re_M}$, is analysed in some detail in Appendix A. In particular, we consider the coupled system given by equations (17) and (18) on scales that are much larger than the resistive scale, but much smaller than the outer forcing scale l of the random motions of the turbulence. In this range one can approximate $\eta_{\rm t}(r)$ and $\alpha(r)$ as power laws. We show quite generally that even in case of helical flows, where large-scale dynamo action is in principle possible, the magnetic spectrum at the kinematic stage is peaked at resistive scales.

Surprisingly, for both a single-scale flow, and for Kolmogorov scaling of the velocity spectra, with maximal kinetic helicity at the forcing scale, we find that helicity is unimportant for the behaviour of the magnetic spectrum at large k. For a helical single scale flow, the magnetic spectrum still scales as the Kazantsev spectrum, $E_{\rm M}(k) \propto k^{3/2}$ at large k. For Kolmogorov scaling of the velocity spectra, with maximally helical forcing, we show in Appendix A that the magnetic spectrum is still peaked at resistive scales; and at large k it is of the form $E_{\rm M}(k) \propto k^s$ with $s \approx 7/6$. Thus, for the kinematic dynamo, even though large-scale fields are being generated due to

the presence of helicity, the magnetic power spectrum is still peaked at resistive scales. Our DNS also suggest such the conclusion that $E_{\rm M}(k) \propto k^s$, with $s > 0$, as can be seen from the spectra shown in Figs 3 and 4. Note also that these conclusions are quite independent of whether the dynamo is predominantly a large-scale or small-scale dynamo, and only depends on there being scale separation between the forcing and resistive scales, as one would obtain for sufficiently large $\mathrm{Re_M}$. We can now ask what this implies for the behaviour of $\overline{B}/B_{\rm rms}$, with $\mathrm{Re_M}$?

Now suppose the magnetic power spectrum increases with k as $E_{\rm M}(k) \propto k^s$ for $k_{\rm f} < k < k_\eta$ and $k_\eta \propto \mathrm{Re_M^\beta}$. Integrating the spectrum over k from $k_{\rm f}$ to k_η, we find for the ratio $(B_{\rm rms}/B_{\rm f})^2 \propto (k_\eta/k_{\rm f})^{s+1} \propto \mathrm{Re_M^{\beta(s+1)}}$, where we have defined the small-scale field at the forcing scale as $B_{\rm f} = (k_{\rm f} M(k_{\rm f}))^{1/2}$. Thus, $(B_{\rm rms}/B_{\rm f}) \propto \mathrm{Re_M^{\beta(s+1)/2}}$. For a single-scale flow, we have $s = 3/2$ and $\beta = 1/2$, and then $B_{\rm rms}/B_{\rm f} \propto \mathrm{Re_M^{5/8}}$. On the other hand, for Kolmogorov scaling of the velocity spectra with $s = 7/6$ and, say, $\beta = 3/4$, we have $(B_{\rm rms}/B_{\rm f}) \propto \mathrm{Re_M^{0.81}}$ scaling. At the same time, we have seen that $\overline{B}/B_s \sim \exp(-k_s/k_m)$ for Type I with $B_s \sim B_{\rm f}$. For Type II, where the large-scale dynamo dominates, one would expect the rms value of $\overline{\boldsymbol{B}}$ to be comparable to $B_{\rm f}$, as would be the case when there is a k^{-1} spectrum (Ruzmaikin & Shukurov 1982) between k_m and $k_{\rm f}$. Combining these arguments, we do expect $\overline{B}/B_{\rm rms}$ to decrease significantly with $\mathrm{Re_M}$, although the exact scaling as $\mathrm{Re_M^{-1/2}}$, or the further scaling as $\mathrm{Re_M^{-3/4}}$, are not yet fully understood.

5 CONCLUSIONS

We have shown here that large-scale dynamo action is obtained in large $\mathrm{Re_M}$ helical turbulence in the kinematic stage, even when a strong small-scale dynamo is also possible. Both large and small scales grow at the same rate, such that the energy spectrum is shape invariant in the kinematic stage. By splitting the magnetic energy spectrum into positively and negatively polarized parts, $E^{\pm}_{\rm M0}$, clear signatures of large-scale fields can be seen at small k as an excess power in $E^{-}_{\rm M0}(k)$ ($E^{+}_{\rm M0}(k)$) if the kinetic helicity at the forcing scale is positive (negative). Evidence for the large-scale mean field $\overline{B}$ is also clearly seen in suitably defined planar averages. This evidence for a mean field in helically driven turbulence is as expected for the standard α^2 mean-field dynamo, and thus allows us to prove the existence of such a mean-field dynamo effect.

The DNS also show that both the amplitude of the large-scale field and the dynamo growth rate increase with increasing fractional helicity. This is as expected and helps to determine the onset of large-scale dynamo action and to distinguish it from that of the small-scale dynamo. As a by-product of our work, we find that for $k_{\rm f}/k_1 = 4$, the $R_{\rm m}^{\rm crit}$ for exciting the small-scale dynamo at small $\mathrm{Pr_M}$ is different from earlier results which were based on smaller scale separation, $k_{\rm f}/k_1 = 1$–2. For example, the threshold magnetic Reynolds number for $\mathrm{Pr_M} = 0.1$ is decreased to a modest value of $R_{\rm m}^{\rm crit} \approx 160$.

The mean field found from the DNS using planar averages, however, decreases with $\mathrm{Re_M}$ as $\mathrm{Re_M^{-1/2}}$ (or possibly faster) in the kinematic stage. Such a decline is obtained both when the small-scale dynamo is dominant (Type I) and also when the large-scale dynamo is dominant, but the small-scale dynamo enslaved to it (Type II). By analysing the Kazantsev model including helicity, this feature is shown to arise due to the fact that the magnetic spectrum $E_{\rm M0}(k)$ for large $\mathrm{Re_M}$, is peaked at the resistive scale, even when helicity is present. Such a rise in $E_{\rm M0}(k)$ with k is also seen in the DNS that we have performed.

This raises the question, does kinematic dynamo theory have any relevance? The answer is yes, because it allows us to *identify* mechanisms that may have a connection with the non-linear regime where the large-scale dynamo becomes dominant and the small-scale power is lost (mode cleaning). First, non-linear simulations of the small-scale dynamo at large $\mathrm{Re_M}$, which have a large enough inertial range show that the non-linear evolution can lead to a significant increase in the magnetic integral scale (Haugen et al. 2004a; Cho & Ryu 2009; Bhat & Subramanian 2013; Eyink et al. 2013). Thus, the effect of the Lorentz force is to bring the power from the resistive scale to scales just smaller than the forcing scale. Also, simulations of the α^2 dynamo in periodic domains, show that the magnetic field becomes ordered on the largest available scales, independently of $\mathrm{Re_M}$, provided small-scale magnetic helicity can be dissipated (Brandenburg 2001, 2009; Candelaresi & Brandenburg 2013). Therefore, the combined action of the Lorentz force to transfer power from resistive scales to larger scales, and small-scale helicity loss from the system, could result in an efficient generation of the large-scale field, even in the presence of the fluctuation dynamo.

For the transfer of power from resistive scales to larger scales to happen, the spectrum must change shape during saturation such that large spatial scales (small k) can still be amplified while small scales (large k) saturate. Recall that all scales grow at the same rate during the kinematic stage. In terms of the potential picture of the Kazantsev model with helicity (Sections 1 and 4), the potential well at the small scale l needs to become shallower due to non-linear effects to allow for only the marginally bound state to exist, while still having sufficient depth at the large scale L, to allow the 'tunnelling free-particle' states to grow. Such local saturation in a related real-space double well potential problem has been found in the context of a spirally forced non-axisymmetric galactic dynamo (Chamandy, Subramanian & Shukurov 2013a,b). There the potential wells are near the galactic centre and the corotation radius of the spiral, so the eigenfunction grows fastest in the central regions, with its tail seeding the growth of the non-axisymmetric magnetic spiral field around corotation. Saturation of the dynamo near the galactic centre still allows for the field to grow around corotation and become significant. Whether such a situation can also be obtained for a double well potential in 'scale' or wavenumber space remains to be determined. It would be of interest to verify this in a non-linear version of the Kazantsev model, where helicity loss can also be built in, and perhaps even more importantly, in high-resolution DNS which can resolve both the small-scale dynamo and have enough scale separation to simultaneously capture the large scales.

ACKNOWLEDGEMENTS

We thank the referee for useful comments which have led to an improvement of the paper. KS thanks Nordita for hospitality during his visit there, which led to this work. This work was supported in part by the European Research Council under the AstroDyn Research Project no. 227952, and the Swedish Research Council grants no. 621-2011-5076 and 2012-5797, as well as the Research Council of Norway under the FRINATEK grant 231444. We acknowledge the allocation of computing resources provided by the Swedish National Allocations Committee at the Center for Parallel Computers at the Royal Institute of Technology in Stockholm and the National Supercomputer Centers in Linköping, the High Performance Computing Center North in Umeå, and the Nordic High Performance Computing Center in Reykjavik.

REFERENCES

Bhat P., Subramanian K., 2013, MNRAS, 429, 2469
Bhat P., Subramanian K., 2014, ApJ, 791, L34
Blackman E. G., Brandenburg A., 2002, ApJ, 579, 359
Boldyrev S., Cattaneo F., Rosner R., 2005, Phys. Rev. Lett., 95, 255001
Brandenburg A., 2001, ApJ, 550, 824
Brandenburg A., 2009, ApJ, 697, 1206
Brandenburg A., 2011, ApJ, 741, 92
Brandenburg A., Subramanian K., 2000, A&A, 361, L33
Brandenburg A., Subramanian K., 2005a, Phys. Rep., 417, 1
Brandenburg A., Subramanian K., 2005b, A&A, 439, 835
Brandenburg A., Dobler W., Subramanian K., 2002, Astron. Nachr., 323, 99
Brandenburg A., Rädler K.-H., Schrinner M., 2008, A&A, 482, 739
Candelaresi S., Brandenburg A., 2013, Phys. Rev. E, 87, 043104
Cattaneo F., Tobias S. M., 2014, ApJ, 789, 70
Chamandy L., Subramanian K., Shukurov A., 2013a, MNRAS, 428, 3569
Chamandy L., Subramanian K., Shukurov A., 2013b, MNRAS, 433, 3274
Cho J., Ryu D., 2009, ApJ, 705, L90
Eyink G. et al., 2013, Nature, 497, 466
Federrath C., Chabrier G., Schober J., Banerjee R., Klessen R. S., Schleicher D. R. G., 2011, Phys. Rev. Lett., 107, 114504
Gent F. A., Shukurov A., Sarson G. R., Fletcher A., Mantere M. J., 2013a, MNRAS, 430, L40
Gent F. A., Shukurov A., Fletcher A., Sarson G. R., Mantere M. J., 2013b, MNRAS, 432, 1396
Gressel O., Ziegler U., Elstner D., Rüdiger G., 2008a, Astron. Nachr., 329, 619
Gressel O., Elstner D., Ziegler U., Rüdiger G., 2008b, A&A, 486, L35
Haugen N. E. L., Brandenburg A., Dobler W., 2004a, Phys. Rev. E, 70, 016308
Haugen N. E. L., Brandenburg A., Mee A. J., 2004b, MNRAS, 353, 947
Iskakov A. B., Schekochihin A. A., Cowley S. C., McWilliams J. C., Proctor M. R. E., 2007, Phys. Rev. Lett., 98, 208501
Kazantsev A. P., 1968, Sov. Phys.–JETP, 26, 1031
Krause F., Rädler K.-H., 1980, Mean-field Magnetohydrodynamics and Dynamo Theory. Pergamon, Oxford
Landau L., Lifshitz E. M., 1987, Fluid Mechanics: Landau and Lifshitz Course of Theoretical Physics, Vol. 6. Pergamon, Oxford
Malyshkin L., Boldyrev S., 2007, ApJ, 671, L185
Malyshkin L., Boldyrev S., 2010, Phys. Rev. Lett., 105, 215002
Moffatt H. K., 1978, Magnetic Field Generation in Electrically Conducting Fluids. Cambridge Univ. Press, Cambridge
Moffatt H. K., 1983, Rep. Prog. Phys., 46, 621
Rogachevskii I., Kleeorin N., 1999, Phys. Rev. E, 59, 3008
Ruzmaikin A., Shukurov A., 1982, Ap&SS, 82, 397407
Schekochihin A. A., Cowley S. C., Maron J. L., McWilliams J. C., 2004, Phys. Rev. Lett., 92, 054502
Schekochihin A. A., Haugen N. E. L., Brandenburg A., Cowley S. C., Maron J. L., McWilliams J. C., 2005, ApJ, 625, L115
Schleicher D. R. G., Schober J., Federrath C., Bovino S., Schmidt W., 2013, New J. Phys., 15, 023017
Schober J., Schleicher D., Bovino S., Klessen R. S., 2012, Phys. Rev. E, 86, 066412
Subramanian K., 1999, Phys. Rev. Lett., 83, 2957
Sur S., Brandenburg A., Subramanian K., 2008, MNRAS, 385, L15
Tobias S. M., Cattaneo F., 2013, Nature, 497, 463
Vainshtein S. I., 1982, Sov. Phys.–JETP, 56, 8684
Vainshtein S.I., Kitchatinov L. L., 1986, J. Fluid Mech., 168, 73
Vainshtein S. I., Cattaneo F., 1992, ApJ, 393, 165

APPENDIX A: THE INFLUENCE OF HELICITY ON SMALL SCALES

The purpose of this appendix is to analyse the behaviour of the coupled system given by equations (17) and (18), on scales that are much larger than the resistive scale, but much smaller than the outer forcing scale l of the random motions or the turbulence. In this range, one can approximate $\eta_t(r)$ and $\alpha(r)$ as power laws. We take quite generally

$$\eta_t(r) = \eta_{T0}\left(\frac{r}{l}\right)^q \quad \text{and} \quad \alpha(r) = \alpha_0\left(\frac{r}{l}\right)^p. \tag{A1}$$

For a single scale flow, we adopt $p = q = 2$. For a Kolmogorov spectrum $E(k) \propto k^{-5/3}$, we can use Richardson scaling for the scale-dependent turbulent diffusion and take $q = 4/3$ (Vainshtein 1982). Suppose further that the flow is driven by a fully helical forcing. Then Brandenburg & Subramanian (2005b) found that the kinetic helicity spectrum also scales as $H_K(k) \propto k^{-5/3}$. Therefore, $\alpha(r = 1/k) \propto \tau(k)(kH_K(k)) \propto r^{4/3}$, where $\tau(k) \propto k^{-2/3}$ is a scale-dependent correlation time. Thus, for a Kolmogorov energy spectrum, assuming also a fully helical velocity field, one could adopt $q = 4/3$, $p = 4/3$. We will discuss both cases below.

Let us define a dimensionless coordinate $z = r/l$, adopt the power-law forms given in equation (A1), and look at eigenmode solutions to equations (17) and (18) of the form $M_L = \exp(\lambda t)\tilde{M}_L(r)$ and $C = \exp(\lambda t)\tilde{C}(r)$. We get

$$\bar{\lambda}\tilde{M}_L(z) = \left(\frac{\eta}{\eta_{T0}} + z^q\right)\tilde{M}_L'' + \left(\frac{4\eta}{\eta_{T0}} + (4+q)z^q\right)\frac{\tilde{M}_L'}{z} + q(3+q)z^{q-2}\tilde{M}_L + 4\bar{\alpha}_0 z^p \tilde{C}(z), \tag{A2}$$

$$\bar{\lambda}\tilde{C}(z) = \left(\frac{\eta}{\eta_{T0}} + z^q\right)\tilde{C}'' + \left(\frac{4\eta}{\eta_{T0}} + (4+2q)z^q\right)\frac{\tilde{C}'}{z} + q(3+q)z^{q-2}\tilde{C} - \bar{\alpha}_0 z^p \tilde{M}_L'' - 2\bar{\alpha}_0(p+2)z^{p-1}\tilde{M}_L' - \bar{\alpha}_0 p(p+3)z^{p-2}\tilde{M}_L. \tag{A3}$$

Here, we have defined a dimensionless growth rate $\bar{\lambda} = l^2\lambda/(2\eta_{T0})$. In the limit $z^q \gg \eta/\eta_{T0}$, or $z \gg z_\eta = (\eta/\eta_{T0})^{1/q}$, one can neglect the resistive terms in equations (A2) and (A3). (Here z_η is the dimensionless resistive scale.) Note that without the mutual coupling due to the α effect, these equations would be scale free in the sense that a transformation of $z \to cz$ leaves equations (A2) and (A3) invariant. The question arises if there still exist scale-free solutions in the presence of an α effect. As power laws are scale free, we examine if equations (A2) and (A3) can have power-law solutions of the form say $\tilde{M}_L = M_0 z^{-\mu}$, $\tilde{C} = C_0 z^{-\nu}$. Substituting this form for $\tilde{M}_L$ and $\tilde{C}$ gives

$$\bar{\lambda}M_0 = [\mu(\mu+1) - \mu(4+q) + q(3+q)]\, M_0 z^{q-2} + 4\bar{\alpha}_0 C_0 z^{p+\mu-\nu}, \tag{A4}$$

$$\bar{\lambda}C_0 = [\nu(\nu+1) - \nu(4+2q) + q(3+q)]\, C_0 z^{q-2} - \bar{\alpha}_0 M_0 z^{p-2+\nu-\mu}\,[\mu(\mu+1) - \mu(4+p) + p(3+p)]. \tag{A5}$$

Thus, a scale-free solution can be obtained if the z dependence drops out in equations (A4) and (A5). To see if this can be obtained, consider now the two cases which we mentioned above. In the case of a single-scale flow with $p = q = 2$, we have $q - 2 = 0$, and the first terms on the right-hand side of equations (A4) and (A5) become z-independent. On the other hand, the exponent of z in the last term of equation (A4) becomes $\mu - \nu + 2$, while that in equation (A5) becomes $\nu - \mu$.

One can get a nearly scale invariant solution if $\mu = \nu$, which implies that equation (A5) becomes z-independent, while $\mu - \nu + 2 = 2$ in equation (A4). Then the exponent of z in the last term in equation (A4) becomes 2 and the z-dependent term in equation (A4) is $\propto z^2 \ll 1$, and thus can be neglected. In this case, the helical part of the correlation completely decouples from the non-helical part of the correlation. Equation (A4) then reduces to that obtained for the standard non-helical small-scale dynamo (Kazantsev 1968; Bhat & Subramanian 2014), and one recovers the Kazantsev spectrum, $E_{\rm M}(k) \propto k^{3/2}$. Thus, even in the presence of helicity in the velocity field, if the fastest growing mode is being driven effectively by a single-scale flow, then helicity is unimportant for the behaviour of the magnetic spectrum at large k!

The nature of the small-z (or large k) solution can be explicitly seen by looking at the solution to the resulting quadratic equation for μ given by equation (A4); cf. Bhat & Subramanian (2014). We get for μ

$$\mu^2 - 5\mu + (10 - \bar{\lambda}) = 0, \quad \text{so } \mu = \frac{5}{2} \pm i\mu_{\rm I}, \tag{A6}$$

where $\mu_I = [4(10 - \bar{\lambda}) - 25]^{1/2}/2$ can be shown to be small (once $\bar{\lambda}$ is determined), and importantly, the real part of μ is $\mu_{\rm R} = 5/2$. From equation (A6), in the range $z_\eta \ll z \ll 1$, $M_{\rm L}$ is then given by

$$M_{\rm L}(z, t) = {\rm e}^{\gamma \tilde{t}} \tilde{M}_0 z^{-\mu_{\rm R}} \cos(\mu_{\rm I} \ln z + \phi), \tag{A7}$$

where $\tilde{M}_0$ and ϕ are constants. Thus $M_{\rm L}$ varies dominantly as $z^{-5/2}$, modulated by the weakly varying cosine factor (both because the phase of the cosine depends on the weakly varying $\ln z$ and because $\mu_{\rm I}$ is small). The magnetic power spectrum is related to $M_{\rm L}$ by

$$E_{\rm M}(k, t) = \int {\rm d}r (kr)^3 M_{\rm L}(r, t) j_1(kr). \tag{A8}$$

The spherical Bessel function $j_1(kr)$ is peaked around $k \sim 1/r$, and a power-law behaviour of $M_{\rm L} \propto z^{-\lambda_{\rm R}}$, for $z_\eta \ll z \ll l$, translates into a power law for the spectrum $E_{\rm M}(k) \propto k^{\lambda_{\rm R}-1}$ at large k (but smaller than the resistive scale, i.e. with $k_\eta = l/z_\eta \gg k \gg 1/l$). As $\lambda_{\rm R} = 5/2$ for a single-scale flow, this implies that the magnetic spectrum is of the Kazantsev form with $E_{\rm M}(k) \propto k^{3/2}$ in k space, as advertised above.

Note that, although the α-effect does not affect the magnetic energy spectrum at large k for a single-scale flow, it is indeed important in driving the current helicity evolution. From equation (A5), we get $C_0 = \bar{\alpha}_0 M_0 (1 - \bar{\lambda}/2\mu)$, which can be used to write $C(r, t)$ explicitly. (We note in passing that the other potentially scale-invariant case would have $\mu - \nu + 2 = 0$. This however implies $\nu = \mu + 2$, and turns out to violate the realizability condition, which in real space requires $\nu \leq \mu + 1$, for power-law correlations/spectra.)

Now consider the other case of Kolmogorov scaling with $q = 4/3$, $p = 4/3$. In this case, the first terms on the right-hand side of equations (A4) and (A5) are proportional to $z^{-2/3}$. On the other hand, the exponent of z in the last term of equation (A4) becomes $4/3 + \mu - \nu$, while that in equation (A5) becomes $-2/3 + \nu - \mu$. Multiplying both equations (A4) and (A5) by $z^{2/3}$, we have

$$\bar{\lambda} M_0 z^{2/3} = [\mu(\mu + 1) - \mu(4 + q) + q(3 + q)] M_0 + 4\bar{\alpha}_0 C_0 z^{2+\mu-\nu} \tag{A9}$$

$$\bar{\lambda} C_0 z^{2/3} = [\nu(\nu + 1) - \nu(4 + 2q) + q(3 + q)] C_0 - \bar{\alpha}_0 M_0 z^{-(\mu-\nu)} [\mu(\mu + 1) - \mu(4 + p) + p(3 + p)]. \tag{A10}$$

Now, for $z \ll 1$, the left-hand side of the above equations will be small and can be neglected. One can then again get a nearly scale invariant solution if $\mu = \nu$, which implies that the right-hand side of equation (A10) becomes z-independent, while $\mu - \nu + 2 = 2$ in equation (A9). Then the exponent of z in the last term in equation (A9) again becomes 2 and the z-dependent term in equation (A9) is $\propto z^2 \ll 1$, and thus can be neglected. In this case, just as in the case of a single-scale flow, the helical part of the correlation completely decouples from the non-helical part of the correlation at small z, in equation (A9). The condition that the resulting homogeneous equation for M_0 has non-trivial solution implies

$$\mu^2 - \frac{13}{3}\mu + \frac{52}{9} = 0. \tag{A11}$$

The resulting quadratic equation has complex conjugate roots, $\mu = \mu_{\rm R} \pm i\mu_{\rm I}$, where now $\mu_{\rm R} = 13/6$ and $\mu_{\rm I} = \sqrt{39}/6$, correspond to the solution for $M_{\rm L}$ given in equation (A7). Although $\mu_{\rm I}$ is now larger and the cosine factor in equation (A7) varies by a larger factor, the power-law envelope $M_{\rm L} \propto z^{-\mu_{\rm R}} \propto z^{-13/6}$ now corresponds to an approximate spectral dependence $E_{\rm M}(k) \propto k^{7/6}$ at large k.

In summary, even in the case of helical flows, where large-scale dynamo action is in principle possible, the magnetic spectrum at the kinematic stage is peaked at resistive scales, with $E_{\rm M}(k) \propto k^s$ at large k, where s ranges from 3/2 (for single-scale flow) to about 7/6 for Kolmogorov scaling of the velocity spectra.

This paper has been typeset from a TEX/LATEX file prepared by the author.

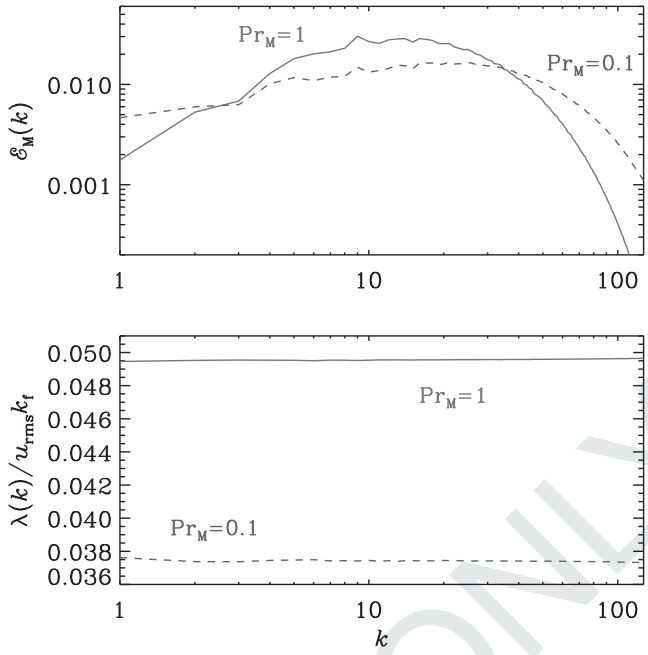

Figure 2. Spectrum of magnetic energy during the kinematic phase for $\mathrm{Pr_M} = 0.1$ (Run F01; blue, dashed lines, $B_{\rm ini} \approx 4 \times 10^{-31}$) and $\mathrm{Pr_M} = 1$ (Run F1; red, solid lines, $B_{\rm ini} \approx 2 \times 10^{-35}$) using $\sigma = 1$ in both cases. The corresponding growth rates as a function of k are given in the bottom panel.

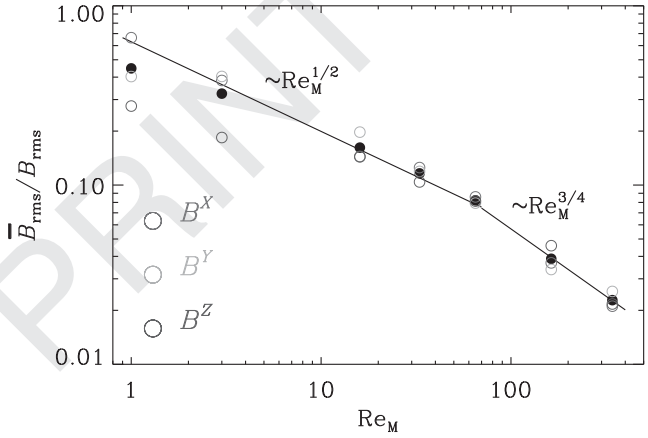

Figure 6. Root-mean-squared value of the mean field relative to that of the total field versus $\mathrm{Re_M}$ for $\mathrm{Pr_M} = 0.1$ and $\sigma = 1$ during the kinematic stage. The filled circles denote the averaged DNS results as an average over the contributions from $\overline{B}^X$, $\overline{B}^Y$, and $\overline{B}^Z$. The straight lines correspond to $0.63\,\mathrm{Re_M^{-1/2}}$ and $1.8\,\mathrm{Re_M^{-3/4}}$ for lower and larger values of $\mathrm{Re_M}$, respectively.

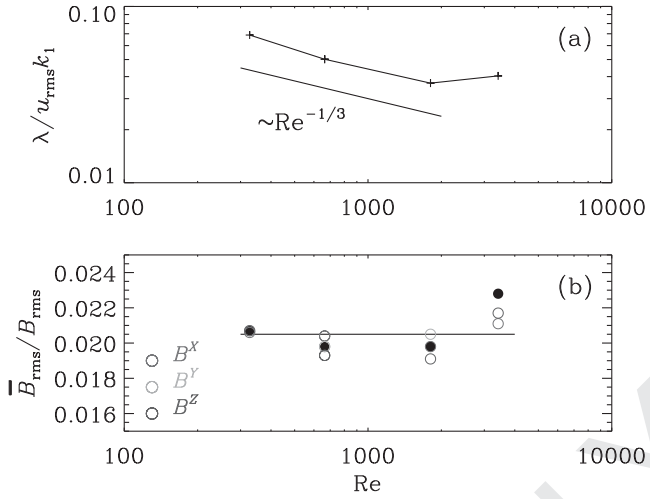

Figure 7. (a) Normalized growth rate versus Re for $\mathrm{Re_M} \approx 330$ and $\sigma = 1$ and (b) root-mean-squared value of the mean field relative to that of the total field during the kinematic stage. Similar to Fig. 6, the filled circles denote the averaged DNS results as an average over the contributions from $\overline{B}^X$, $\overline{B}^Y$, and $\overline{B}^Z$. The horizontal line is shown for reference.

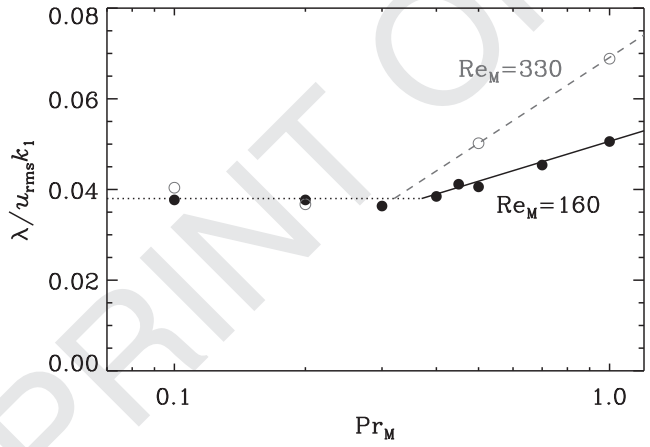

Figure 9. Normalized growth rate versus $\mathrm{Pr_M}$ for $\sigma = 1$, $\mathrm{Re_M} \approx 160$ (Runs F01–F1; solid black line with filled symbols) or ≈330 (Runs G01–G1; dashed red line with open symbols) and varying values of $\mathrm{Re} = \mathrm{Re_M}/\mathrm{Pr_M}$. The dotted line indicates the growth rate for a predominantly large-scale dynamo.

List of astronomical key words (updated 2013 July)

This list is common to *Monthly Notices of the Royal Astronomical Society, Astronomy and Astrophysics*, and *The Astrophysical Journal*. In order to ease the search, the key words are subdivided into broad categories. No more than *six* subcategories altogether should be listed for a paper.

The subcategories in boldface containing the word 'individual' are intended for use with specific astronomical objects; these should never be used alone, but always in combination with the most common names for the astronomical objects in question. Note that each object counts as one subcategory within the allowed limit of six.

The parts of the key words in italics are for reference only and should be omitted when the key words are entered on the manuscript.

General

editorials, notices
errata, addenda
extraterrestrial intelligence
history and philosophy of astronomy
miscellaneous
obituaries, biographies
publications, bibliography
sociology of astronomy
standards

Physical data and processes

acceleration of particles
accretion, accretion discs
asteroseismology
astrobiology
astrochemistry
astroparticle physics
atomic data
atomic processes
black hole physics
chaos
conduction
convection
dense matter
diffusion
dynamo
elementary particles
equation of state
gravitation
gravitational lensing: strong
gravitational lensing: weak
gravitational lensing: micro
gravitational waves
hydrodynamics
instabilities
line: formation
line: identification
line: profiles
magnetic fields
magnetic reconnection
(magnetohydrodynamics) MHD
masers
molecular data
molecular processes
neutrinos
nuclear reactions, nucleosynthesis, abundances
opacity
plasmas
polarization
radiation: dynamics
radiation mechanisms:general
radiation mechanisms: non-thermal
radiation mechanisms: thermal
radiative transfer
relativistic processes
scattering
shock waves
solid state: refractory
solid state: volatile
turbulence
waves

Astronomical instrumentation, methods and techniques

atmospheric effects
balloons
instrumentation: adaptive optics
instrumentation: detectors
instrumentation: high angular resolution
instrumentation: interferometers
instrumentation: miscellaneous
instrumentation: photometers
instrumentation: polarimeters
instrumentation: spectrographs
light pollution
methods: analytical
methods: data analysis
methods: laboratory: atomic
methods: laboratory: molecular
methods: laboratory: solid state
methods: miscellaneous
methods: numerical
methods: observational
methods: statistical
site testing
space vehicles
space vehicles: instruments
techniques: high angular resolution
techniques: image processing
techniques: imaging spectroscopy
techniques: interferometric
techniques: miscellaneous
techniques: photometric
techniques: polarimetric
techniques: radar astronomy
techniques: radial velocities

techniques: spectroscopic
telescopes

Astronomical data bases

astronomical data bases: miscellaneous
atlases
catalogues
surveys
virtual observatory tools

Astrometry and celestial mechanics

astrometry
celestial mechanics
eclipses
ephemerides
occultations
parallaxes
proper motions
reference systems
time

The Sun

Sun: abundances
Sun: activity
Sun: atmosphere
Sun: chromosphere
Sun: corona
Sun: coronal mass ejections (CMEs)
Sun: evolution
Sun: faculae, plages
Sun: filaments, prominences
Sun: flares
Sun: fundamental parameters
Sun: general
Sun: granulation
Sun: helioseismology
Sun: heliosphere
Sun: infrared
Sun: interior
Sun: magnetic fields
Sun: oscillations
Sun: particle emission
Sun: photosphere
Sun: radio radiation
Sun: rotation
(Sun:) solar–terrestrial relations
(Sun:) solar wind
(Sun:) sunspots
Sun: transition region
Sun: UV radiation
Sun: X-rays, gamma-rays

Planetary systems

comets: general
comets: individual: . . .
Earth
interplanetary medium
Kuiper belt: general
Kuiper belt objects: individual: . . .
meteorites, meteors, meteoroids
minor planets, asteroids: general
minor planets, asteroids: individual: . . .
Moon
Oort Cloud
planets and satellites: atmospheres
planets and satellites: aurorae
planets and satellites: composition
planets and satellites: detection
planets and satellites: dynamical evolution and stability
planets and satellites: formation
planets and satellites: fundamental parameters
planets and satellites: gaseous planets
planets and satellites: general
planets and satellites: individual: . . .
planets and satellites: interiors
planets and satellites: magnetic fields
planets and satellites: oceans
planets and satellites: physical evolution
planets and satellites: rings
planets and satellites: surfaces
planets and satellites: tectonics
planets and satellites: terrestrial planets
planet–disc interactions`
planet–star interactions
protoplanetary discs
zodiacal dust

Stars
stars: abundances
stars: activity
stars: AGB and post-AGB
stars: atmospheres
(stars:) binaries *(including multiple)*: close
(stars:) binaries: eclipsing
(stars:) binaries: general
(stars:) binaries: spectroscopic
(stars:) binaries: symbiotic
(stars:) binaries: visual
stars: black holes
(stars:) blue stragglers
(stars:) brown dwarfs
stars: carbon
stars: chemically peculiar
stars: chromospheres
(stars:) circumstellar matter
stars: coronae
stars: distances
stars: dwarf novae
stars: early-type
stars: emission-line, Be
stars: evolution
stars: flare
stars: formation
stars: fundamental parameters
(stars:) gamma-ray burst: general
(stars:) **gamma-ray burst: individual: . . .**
stars: general
(stars:) Hertzsprung–Russell and colour–magnitude diagrams
stars: horizontal branch
stars: imaging
stars: individual: . . .

stars: interiors
stars: jets
stars: kinematics and dynamics
stars: late-type
stars: low-mass
stars: luminosity function, mass function
stars: magnetars
stars: magnetic field
stars: massive
stars: mass-loss
stars: neutron
(stars:) novae, cataclysmic variables
stars: oscillations *(including pulsations)*
stars: peculiar *(except chemically peculiar)*
(stars:) planetary systems
stars: Population II
stars: Population III
stars: pre-main-sequence
stars: protostars
(stars:) pulsars: general
(stars:) **pulsars: individual: . . .**
stars: rotation
stars: solar-type
(stars:) starspots
stars: statistics
(stars:) subdwarfs
(stars:) supergiants
(stars:) supernovae: general
(stars:) **supernovae: individual: . . .**
stars: variables: Cepheids
stars: variables: δ Scuti
stars: variables: general
stars: variables: RR Lyrae
stars: variables: S Doradus
stars: variables: T Tauri, Herbig Ae/Be
(stars:) white dwarfs
stars: winds, outflows
stars: Wolf–Rayet

Interstellar medium (ISM), nebulae

ISM: abundances
ISM: atoms
ISM: bubbles
ISM: clouds
(ISM:) cosmic rays
(ISM:) dust, extinction
ISM: evolution
ISM: general
(ISM:) H II regions
(ISM:) Herbig–Haro objects
ISM: individual objects: . . .
(except planetary nebulae)
ISM: jets and outflows
ISM: kinematics and dynamics
ISM: lines and bands
ISM: magnetic fields
ISM: molecules
(ISM:) planetary nebulae: general
(ISM:) **planetary nebulae: individual: . . .**
(ISM:) photodissociation region (PDR)
ISM: structure
ISM: supernova remnants

The Galaxy

Galaxy: abundances
Galaxy: bulge
Galaxy: centre
Galaxy: disc
Galaxy: evolution
Galaxy: formation
Galaxy: fundamental parameters
Galaxy: general
(Galaxy:) globular clusters: general
(Galaxy:) **globular clusters: individual: . . .**
Galaxy: halo
Galaxy: kinematics and dynamics
(Galaxy:) local interstellar matter
Galaxy: nucleus
(Galaxy:) open clusters and associations: general
(Galaxy:) **open clusters and associations: individual: . . .**
(Galaxy:) solar neighbourhood
Galaxy: stellar content
Galaxy: structure

Galaxies

galaxies: abundances
galaxies: active
(galaxies:) BL Lacertae objects: general
(galaxies:) **BL Lacertae objects: individual: . . .**
galaxies: bulges
galaxies: clusters: general
galaxies: clusters: individual: . . .
galaxies: clusters: intracluster medium
galaxies: distances and redshifts
galaxies: dwarf
galaxies: elliptical and lenticular, cD
galaxies: evolution
galaxies: formation
galaxies: fundamental parameters
galaxies: general
galaxies: groups: general
galaxies: groups: individual: . . .
galaxies: haloes
galaxies: high-redshift
galaxies: individual: . . .
galaxies: interactions
(galaxies:) intergalactic medium
galaxies: irregular
galaxies: ISM
galaxies: jets
galaxies: kinematics and dynamics
(galaxies:) Local Group
galaxies: luminosity function, mass function
(galaxies:) Magellanic Clouds
galaxies: magnetic fields
galaxies: nuclei
galaxies: peculiar
galaxies: photometry
(galaxies:) quasars: absorption lines
(galaxies:) quasars: emission lines
(galaxies:) quasars: general
(galaxies:) **quasars: individual: . . .**
(galaxies:) quasars: supermassive black holes
galaxies: Seyfert

galaxies: spiral
galaxies: starburst
galaxies: star clusters: general
galaxies: star clusters: individual: . . .
galaxies: star formation
galaxies: statistics
galaxies: stellar content
galaxies: structure

Cosmology

(cosmology:) cosmic background radiation
(cosmology:) cosmological parameters
cosmology: miscellaneous
cosmology: observations
cosmology: theory
(cosmology:) dark ages, reionization, first stars
(cosmology:) dark energy
(cosmology:) dark matter
(cosmology:) diffuse radiation
(cosmology:) distance scale
(cosmology:) early Universe
(cosmology:) inflation
(cosmology:) large-scale structure of Universe
(cosmology:) primordial nucleosynthesis

Resolved and unresolved sources as a function of wavelength

gamma-rays: diffuse background
gamma-rays: galaxies
gamma-rays: galaxies: clusters
gamma-rays: general
gamma-rays: ISM
gamma-rays: stars
infrared: diffuse background
infrared: galaxies
infrared: general
infrared: ISM
infrared: planetary systems
infrared: stars
radio continuum: galaxies
radio continuum: general
radio continuum: ISM
radio continuum: planetary systems
radio continuum: stars
radio lines: galaxies
radio lines: general
radio lines: ISM
radio lines: planetary systems
radio lines: stars
submillimetre: diffuse background
submillimetre: galaxies
submillimetre: general
submillimetre: ISM
submillimetre: planetary systems
submillimetre: stars
ultraviolet: galaxies
ultraviolet: general
ultraviolet: ISM
ultraviolet: planetary systems
ultraviolet: stars
X-rays: binaries
X-rays: bursts
X-rays: diffuse background
X-rays: galaxies
X-rays: galaxies: clusters
X-rays: general
X-rays: individual: . . .
X-rays: ISM
X-rays: stars